Metabolic impact of heterologous protein production in *Pseudomonas putida*: Insights into carbon and energy flux control

Philippe Vogeleer[1], Pierre Millard[1,2], Ana-Sofia Ortega Arbulú[4], Katharina Pflüger-Grau[4], Andreas Kremling[4] and Fabien Létisse[1,3]*

[1]Toulouse Biotechnology Institute, Université de Toulouse, INSA, UPS, Toulouse, France.

[2]MetaToul-MetaboHUB, National Infrastructure of Metabolomics and Fluxomics, Toulouse, France.

[3]Present address: Institut de Pharmacologie et de Biologie Structurale (IPBS), Université de Toulouse, CNRS, Université Toulouse III - Paul Sabatier (UT3), Toulouse, France

[4]Technical University Munich, TUM School of Engineering and Design, Department of Energy and Process Engineering, Systems Biotechnology, Germany

***Corresponding author**

Fabien Létisse : fabien.letisse@univ-tlse3.fr

Abstract

For engineered microorganisms, the expression of heterologous proteins that are often useless to host cells represents a burden on resources, which have to be shared with normal cellular processes. Within a certain metabolic leeway, this competitive process has no impact on growth. However, once this leeway, or free capacity, is fully utilized, the extra load becomes a metabolic burden that inhibits cellular processes and triggers a broad cellular response, reducing cell growth and often hindering the production of heterologous proteins.

In this study, we sought to characterize the metabolic rearrangements occurring in the central metabolism of *Pseudomonas putida* at different levels of metabolic load. To this end, we constructed a *P. putida* KT2440 strain that expressed two genes encoding fluorescent proteins, one in the genome under constitutive expression to monitor the free capacity, and the other on an inducible plasmid to probe heterologous protein production. We found that metabolic fluxes are profoundly reshuffled, notably at the level of periplasmic pathways, as soon as the metabolic load exceeds the free capacity. Heterologous protein production leads to the decoupling of anabolism and catabolism, resulting in large excess energy production relative to the requirements of protein biosynthesis. Finally, heterologous protein production was found to exert a stronger control on carbon fluxes than on energy fluxes, indicating that the flexible nature of *P. putida*'s central metabolic network is solicited to sustain energy production.

Highlights : (3 – 5 bullet points/85 characters)

Heterologous protein production in *P. putida* reshuffles the periplasmic metabolism.

Increased protein production progressively decouples catabolism from anabolism.

Protein production exerts a stronger control on energy than on carbon fluxes.

Glucose is directed towards ATP production to meet the elevated energy demands.

Keywords: Heterologous protein production, *P. putida*, fluxomics, metabolic control, metabolic burden, resource allocation

43 **1. Introduction**

44 *Pseudomonas putida* is widely regarded as a valuable workhorse for white biotechnology due
45 to its combination of rapid growth, minimal nutrient requirements, and versatile metabolism
46 (Nikel and de Lorenzo, 2018). Its resistance to toxic compounds, organic solvents and to
47 variations in pH and temperature also make it attractive for industrial applications. Moreover,
48 *P. putida* lacks the virulence factors commonly found in the genome of other *Pseudomonas*
49 species (*i.e.* type III secretion system and endotoxin A) (Udaondo et al., 2016). Its ability to
50 produce endogenous biopolymers, such as polyhydroxyalkanoates (PHA) and non-ribosomal
51 peptides (Loeschcke and Thies, 2015) is widely exploited. It is also used in bioremediation
52 processes, as it produces various enzymes that degrade xenobiotic aromatic compounds (de
53 Lorenzo, 2008; Poblete-Castro et al., 2017). This ability to degrade aromatic compounds and
54 its high intrinsic resistance to metabolic and physiological stresses differentiates *P. putida*
55 from other bacterial species used in synthetic biology such as *Escherichia coli* and *Bacillus*
56 *subtilis* (Nikel et al., 2014), and makes *P. putida* a promising organism for biotechnological
57 applications.

58 However, biotechnological production is often limited by cellular capacity (Ceroni et al., 2015)
59 and in engineered cells, the heterologous expression of proteins represents an unnatural load,
60 which consumes energy and cellular resources, such as ribosomes, polymerases and
61 metabolites. Cells have a certain metabolic leeway, which we call their *free capacity*, that
62 allows them to produce heterologous proteins without reducing their growth rate. Any
63 additional load, however, becomes a burden and the growth rate decreases (Borkowski et al.,
64 2016). The central metabolism responds by providing precursors, and chemical and redox

65 energy for the implemented task, but this also triggers stress-induced mechanisms related to
66 protein production (Wittmann et al., 2007).

67 *P. putida*'s metabolism is characterized by its particular central carbon network (Figure 1). At
68 the periplasmic level, glucose is primarily directly oxidized to gluconate with a smaller fraction
69 being converted to 2-ketogluconate (2-KG). Once internalized into the cytoplasm by their
70 respective transporters, these metabolites are converted into 6-phosphogluconate (6-PG)
71 either by gluconate kinase (GntK) or *via* the 2-KG bypass, by the activity of 2-KG kinase (KguK)
72 and 2-KG-6-P reductase (KguD) (del Castillo et al., 2007; Vicente and Cánovas, 1973).
73 Furthermore, the classical Embden–Meyerhof–Parnas (EMP) pathway is nonfunctional
74 because of the absence of phosphofructokinase, which normally converts fructose-6-
75 phosphate to fructose-1,6-biP. As a consequence, carbon is processed mainly *via* the Entner-
76 Doudoroff (ED) pathway and partially *via* the pentose phosphate (PP) pathway (Nikel et al.,
77 2015). Compared to the EMP pathway, commonly known as glycolysis, the oxidation of one
78 mole of glucose into two pyruvates through the ED pathway yields less ATP (one mole only)
79 but an equal amount of catabolic and anabolic reducing power (one NADH or one NADPH
80 molecule, respectively) instead of two NADHs. Remarkably, NADPH formation is also boosted
81 by the recycling of the glyceraldehyde-3-phosphate (GAP) formed from glucose in the ED
82 pathway to hexose-phosphate, and the combined action of enzymes from the ED pathway,
83 the EMP pathway (in the gluconeogenic direction) and the PP pathway, in what is collectively
84 known as the EDEMP cycle (Kohlstedt and Wittmann, 2019; Nikel et al., 2015). The EDEMP
85 cycle enables *P. putida* to adjust NADPH production to meet anabolic demands and provides
86 the intrinsic resistance to oxidative stress (Kim and Park, 2014). The cyclic architecture of *P.*
87 *putida*'s metabolism thus supports stress resistance alongside oxidative energy production. In
88 the context of biotechnology applications (Volke et al., 2020), an important question is how

89 the specific features of *P. putida*'s central metabolism allow the bacteria to cope with the
90 metabolic load incurred by protein overproduction.

91 The aim of this study was to characterize the rearrangements in *P. putida*'s central metabolism
92 at different levels of protein overproduction. Following Ceroni *et al*. (2015), we constructed a
93 *P. putida* KT2440 strain that i) constitutively expressed the *mCherry* gene to monitor cellular
94 capacity and ii) carried a plasmid encoding maltose-binding protein (MBP) fused to fluorescent
95 eGFP for better detection under the control of an inducible promoter. Protein production was
96 tuned by varying the concentrations of the inducer, and quantified by measuring the level of
97 green fluorescence. The metabolic response to the different levels of metabolic burden
98 induced by gradually increasing heterologous protein production was investigated by
99 measuring bacterial growth and carbon and energy fluxes. Comparisons between metabolic
100 flux maps obtained under induced and non-induced conditions provide insights into the flux
101 rearrangements within the central metabolism caused by protein production.

102 **2. Material and Methods**

103 **2.1 Strains and plasmids**

104 *P. putida* and *E. coli* strains were cultivated at 30 °C or 37 °C, respectively, in either LB or M9
105 minimal medium (Miller, 1974) with glucose as C-source. Strains were stored in cryotubes at
106 -80 °C, in LB medium containing 15 % glycerol (v/v).

107 ***Construction of the capacity monitor strain, P. putida CAP.*** *P. putida* CAP was constructed by
108 inserting the *mCherry* gene into the chromosome of *P. putida* KT2440 under the control of a
109 constitutive promoter. The promoter of the *lac*-operon of *E. coli* was chosen, as this promoter
110 is only regulated by its genomic context (Oehler, 2009). The fragment containing the *mCherry*

111 gene under the control of *lacIp* was cloned into pTn7-M (Zobel et al., 2015) choosing SpeI and
112 SacI restriction sites in *E. coli* DH5α λpir. The resulting pTn7-M_lacIp-*mCherry* vector was
113 introduced into *P. putida* KT2440 by quadruple conjugation with *E. coli* DH5α λpir (pTn7-
114 M_lacIp-*mCherry*) as donor, *E. coli* HB101 (pRK600) as a helper strain for conjugation, *E. coli*
115 DH5α (pTnS1) to provide transposase, and *P. putida* KT2440 as recipient (Choi and Schweizer,
116 2006; Zobel et al., 2015). The resulting *P. putida* KT2440 *attTn7::lacIp-mCherry* strain, referred
117 to as *P. putida* CAP (for capacity), was selected by growth on citrate and resistance towards
118 gentamycin. The correct integration of *lacIp-mCherry* was confirmed by amplification of a
119 fragment spanning the *lacIp-mCherry* region and sequencing.

120 ***Construction of the burden plasmid pSEVA438-MBPeGFP*.** The *malE* gene was genetically
121 fused *via* a GlySer-linker (GGGGS) to the N-terminus of *eGFP* by overlap extension PCR.
122 Primers were designed to remove the periplasmic signal sequence of *malE* to avoid
123 extracellular transport of the heterologous protein. eGFP was tagged on the C-terminus with
124 a polyhistidine-tag (6xHis-tag), yielding the MBPeGFP fragment. The fragment was ligated into
125 pSEVA438 using EcoRI and SpeI as restriction sites and the resulting plasmid, pSEVA438-
126 MBPeGFP, was transferred to *E. coli* DH5α λpir using the TSS method (Chung et al., 1989).
127 Positive clones were then selected by streptomycin resistance. After verification of
128 pSEVA438_MBPeGFP by sequencing, the plasmid was transferred to *P. putida* CAP by
129 triparental mating (de Lorenzo and Timmis, 1994), yielding *P. putida* CAP
130 (pSEVA438_MBPeGFP) (Figure 2A).

131 **2.2 Media and preculture conditions.** For each experiment, the strains were first streaked
132 onto LB agar plates containing 200 µg/mL streptomycin and incubated overnight at 30 °C.
133 Then, 3 mL of LB medium with 200 µg/mL streptomycin were inoculated from a single isolated

134 colony and the cultures were incubated for 8 to 16 h at 30 °C and 200 rpm in an orbital shaker
135 (Inova 4230, New Brunswick Scientific, New Brunswick, NJ, USA). Cells were first diluted
136 (1/100) in 50 mL of M9 medium containing 17.4 g/L $Na_2HPO_4 \cdot 12H_2O$, 3.0 g/L KH_2PO_4, 2.0 g/L
137 NH_4Cl, 0.5 g/L NaCl, 0.5 g/L $MgSO_4$, and 3.3 mg/L $CaCl_2$, and 1 mL of a trace element solution
138 containing 15 mg/L $Na_2EDTA \cdot 2H_2O$, 4.5 mg/L $ZnSO_4 \cdot 7H_2O$, 0.3 mg/L $CoCl_2 \cdot 6H_2O$, 1 mg/L
139 $MnCl_2 \cdot 4H_2O$, 1 mg/L H_3BO_3, 0.4 mg/L $Na_2MoO \cdot 2H_2O$, 3 mg/L $FeSO_4 \cdot 7H_2O$,0.3 mg/L $CuSO_4 \cdot$
140 $5H_2O$. M9 preculture medium was supplemented with 3 $g \cdot L^{-1}$ glucose for flux analysis, or with
141 3 $g \cdot L^{-1}$ of a glucose mixture containing 80 % $^{13}C_1$-labeled glucose and 20 % U-$^{13}C_6$-labeled
142 glucose (Eurisotop, Saint Aubin, France). The glucose, $MgSO_4$ and trace element solutions
143 were sterilized by filtration (Minisart 0.2-μm syringe filter; Sartorius, Göttingen, Germany) and
144 other solutions were autoclaved. Cells were incubated in a 250 mL baffled flask at 30 °C and
145 shaken at 200 rpm. Exponentially growing cells were harvested by centrifugation (Sigma 3-
146 18K centrifuge, Sigma-Aldrich, Seelze, Germany) at 5,000 *g* for 15 min at room temperature,
147 washed twice in fresh medium without glucose, and this inoculum was used to inoculate
148 microtiter plates or bioreactors. A 0.5 M stock solution of inducer was prepared by solubilizing
149 3-methyl-benzoate (3-MB) (Sigma-Aldrich, St Louis, MO, USA) in 0.5 M NaOH.

150 **2.3 Batch culture in microtiter plate.** *P. putida* KT2440 CAP (pSEVA438_MBPeGFP) inoculum
151 was diluted to an optical density at 600 nm (OD_{600}) of 0.07 (Genesys 6 spectrophotometer,
152 Thermo, Carlsbad, CA, USA) in 5 mL M9 medium containing 3 $g \cdot L^{-1}$ glucose and 200 µg/mL
153 streptomycin and supplemented with 50 µL of different inducer concentrations (0, 0.5, 1, 2.5,
154 5, 10, 25, 50, 100, 250, 500, 1000 µM) prepared from a 0.5 M stock solution of 3-MB (Sigma-
155 Aldrich, St Louis, MO, USA) solubilized in a 0.5 M NaOH solution and filtered through a 0.2 μm
156 filter for sterilization (Minisart 0.2 µm syringe filter; Sartorius, Göttingen, Germany). These
157 dilutions were then inoculated (100 µL) in triplicate into a 96 well microtiter plate (Sarstedt,

158 Nümbrecht, Germany) and incubated at 30 °C in a plate reader (CLARIOstar^{Plus}, BMG Labtech,
159 Ortenberg, Germany). The optical density at 600 nm (OD_{600}) and fluorescence of GFP
160 (excitation wavelength, λex, 470 nm; emission wavelength 1, λem1, 515 nm),
161 autofluorescence (λex, 470 nm; λem, 580 nm) and *mCherry* (λex, 570 nm; λem, 620 nm) were
162 measured every 20 min for 48 h under continuous 200 rpm double orbital shaking. Three
163 independent biological replicates were analyzed.

164 **2.4 Batch culture in bioreactors.** *P. putida* KT2440 WT and *P. putida* CAP
165 (pSEVA438_MBPeGFP) were grown in a 500 mL bioreactor (my-Control, Applikon
166 Biotechnology INC, Sunnyvale, CA, USA) containing 300 mL of bioreactor-adapted M9 medium
167 containing 4.0 g·L^{-1} NH_4Cl, 2.0 g·L^{-1} KH_2PO_4, 0.5 g·L^{-1} NaCl, 0.5 g·L^{-1} $MgSO_4$, 4.3 mg·L^{-1} $CaCl_2$,
168 and 1 mL of the trace element solution supplemented with 10 g·L^{-1} glucose. For flux analysis,
169 ^{12}C-glucose was replaced by a 10 g·L^{-1} mixture of 80 % (mol/mol) $^{13}C_1$-labeled glucose and 20
170 % (mol/mol) U-$^{13}C_6$-labeled glucose (with a ^{13}C purity of 99 %; Eurisotop, Saint Aubin, France).
171 The pH was maintained at 7.0 ± 0.1 by automatically adding 14% (g/g) ammonia (VWR,
172 Fontenay-sous-Bois, France) or 10 % (g/g) phosphoric acid (PanReac AppliChem, Barcelona,
173 Spain) and the temperature was set to 30 °C. Adequate aeration of the culture was achieved
174 by automatically controlling the stirrer speed and the gas flow to maintain > 30 % oxygen
175 saturation. Streptomycin (200 µg/mL) was added to the *P. putida* CAP (pSEVA438_MBPeGFP)
176 culture. The inducer for protein production was added before cell inoculation, at 10 µM or 1
177 mM from a 0.5 M stock solution of 3-MB (Sigma-Aldrich, St Louis, MO, USA) solubilized in 0.5
178 M NaOH. Foaming was avoided by manually adding 50 µL of antifoam 204 (Sigma-Aldrich, S^t
179 Louis, MO, USA) before inoculation and when required during growth. The bioreactor was
180 inoculated to an OD_{600} of 0.15. Depending on the culture time, 1.0 to 2.5 mL of culture were
181 withdrawn from the bioreactor every 0.5 to 1 h to monitor the OD_{600}, fluorescence, and

182 protein and metabolite contents of the culture. Cell dry weight (CDW) was determined by
183 filtering 5 mL of cells grown in M9 supplemented with glucose at OD_{600} 1.0, 1.5 and 2.0 on
184 preweighed membrane filters (Sartorius 0.2 µm, 47 mm, Goettingen, Germany) under vacuum
185 filtration. The filters were then washed with a 0.9 % NaCl solution, incubated at 80 °C and
186 weighed every 24 h until a constant weight was reached. Under our laboratory conditions, the
187 OD_{600} CDW correlation for *P. putida* was CDW [$g \cdot L^{-1}$] = 0.57 ± 0.01 × OD_{600}.

188 **2.5 Fluorescence data processing.** The green fluorescence specifically emitted by eGFP was
189 measured in relative light units (RLU_{GFP}) using a procedure similar to the one described by
190 Lichten et al. (2014). Both specific and non-specific eGFP fluorescence signals were measured
191 at λem = 515 and 580 nm to calculate the autofluorescence signal, which was then subtracted
192 to avoid overestimating heterologous protein production. The ratio of autofluorescence at
193 515 nm and 580 nm was calculated for a KT2440 WT culture, yielding $r_a = RLU_{515}/RLU_{580}$ = 2.479
194 (R^2=0.999; Figure S1A supplementary data). Based on these data, the autofluorescence of *P.*
195 *putida* CAP (pSEVA438_MBPeGFP) was determined for each measurement and subtracted
196 from the level of green fluorescence, yielding the amount of fluorescence specific to the
197 heterologous protein, $RLU_{GFP} = RLU_{515} - r_a x RLU_{580}$, (Lichten et al., 2014). The overlap between
198 the autofluorescence signal of the cells and the fluorescence emitted by mCherry at 620 nm
199 was negligible.

200 **2.6 Purification of heterologous protein**. The heterologous protein MBPeGFP was purified
201 using NEBExpress Ni spin columns (NEB**,** Ipswich, MA, USA) according to manufacturer
202 recommendations. Briefly, 50 mL of *P. putida* CAP (pSEVA438_MBPeGFP) culture induced with
203 1 mM of 3-MB (Sigma-Aldrich, St Louis, MO, USA) were extracted from a bioreactor at OD_{600}
204 of 2.25, harvested at 5,000 *g* for 15 min, and stored at -80 °C until further analysis. Frozen cell

205 pellets were resuspended in 4 mL of IMAC buffer (NEB**,** Ipswich, MA, USA) on ice and dispersed
206 using an ultrasonic disruptor (Sonics, VibraCell^{TM}, Newtown, CT, USA) in 9 sonication cycles
207 (20 s ON, 30 s OFF; power amplitude, 20 %) with a pause of 60 s in between. Cell debris was
208 removed by centrifugation (15 min at 16,100 *g*). Protein purification was then carried out
209 following the manufacturer's protocol. After adding 200 µL of elution buffer containing 50 mM
210 imidazole, the concentration of MBPeGFP was measured with a bicinchoninic acid (BCA) assay
211 using bovine serum albumin (BSA) dilutions ranging from 0 to 206.25 µg/mL to establish a
212 standard curve (Figure S1B supplementary data). Purified MBPeGFP was two-fold serially
213 diluted. BSA standard and purified protein (25 µL) were each added in triplicate to a microtiter
214 plate (Sarstedt, Nümbrecht, Germany) and 200 µL of a 50:1 mixture of BCA and copper(II)
215 sulfate solutions (Sigma-Aldrich, St Louis, MO, USA) was added to each well containing a
216 sample. The plate was incubated for 30 min at 37 °C, then left to cool at room temperature
217 for 5 min before absorbance was measured at 562 nm with a plate reader (CLARIOstar^{Plus},
218 BMG Labtech, Ortenberg, Germany). The final concentration of purified protein was 1076
219 µg/mL. This stock solution was then diluted (at concentrations of 175, 150, 125, 100, 75, 50
220 µg/mL) and mixed with 4X Laemmli buffer (Biorad, Hercules, CA, USA) containing 1 % β-
221 mercaptoethanol for SDS-PAGE calibration, as detailed below (Figure S1C and D
222 supplementary data).

223 **2.7 Heterologous protein quantification by SDS-PAGE and fluorescence correlation factor.**
224 Bioreactor culture samples (60 µL) were extracted at an OD_{600} of 1 to 4, diluted to an OD_{600} of
225 1, mixed with 4X Laemmli buffer (Biorad, Hercules, CA, USA) containing 1 % β-
226 mercaptoethanol and stored at −20 °C until analysis. After denaturation for 5 min at 95 °C, 8
227 µL of cellular extract and dilutions of purified protein (at 175, 150, 125, 100, 75, 50 µg/mL)
228 were loaded onto a 12.5 % SDS-PAGE gel and separated at 160 V for 70 min in a mini-protean

229 tetra cell (Biorad, Hercules, CA, USA) using Tris-glycine-SDS running buffer. The gels were
230 washed once with distilled water and stained with InstantBlue® Coomassie Protein Stain
231 (Abcam, Cambridge, UK). The gels were viewed using a ChemiDOC XRS molecular imager
232 (Biorad, Hercules, CA, USA) (Figure S1C supplementary data) and the images were analyzed
233 using Image Lab v6.0.1 (Biorad, Hercules, CA, USA). Brightness and contrast were adjusted
234 automatically using the software. Lanes and bands were identified manually. The lane profile
235 tool was used to quantify the peak area that corresponded as precisely as possible to the
236 protein band. The resulting calibration curve for MBPeGFP (Figure S1D supplementary data)
237 was used to estimate its concentration in the samples (Figure S1E supplementary data). A
238 correlation factor between the amount of green fluorescence ($RLU_{MBPeGFP}$) emitted by the
239 sample and the protein concentration was calculated from the slope of the curve (Fluo factor
240 7.25×10^{-9} - 0.0007, $R^2 = 0.954$). This was used to convert the levels of green fluorescence
241 measured in other samples into MBPeGFP protein concentrations.

242 **2.8 Quantification of extracellular metabolites by NMR.**

243 Glucose, gluconate and 2-KG were identified and quantified by nuclear magnetic resonance
244 (NMR). Culture samples (1 mL) were collected every 0.5 to 1 h during growth, centrifuged at
245 14,500 *g* for 3 min, and the supernatants were stored at −20 °C until analysis. The supernatants
246 (180 µL) were mixed with 20 µL of an internal standard consisting of 10 mM deuterated
247 trimethylsilylpropanoic acid (TSP-d4) diluted in D_2O. Proton NMR spectra were recorded on
248 an Avance III 500-MHz spectrometer equipped with a 5-mm z-gradient TXI (^1H, ^{13}C, ^{31}P) probe
249 (Brucker, Rheinstatten, Germany). Quantitative ^1H NMR analysis was performed at 286 K,
250 using a zgpr30 sequence with a recycle delay of 10 s, and presaturation at 4.7 ppm for water
251 suppression. Thirty-two scans were accumulated (32k data points with a spectral width of 10

252 ppm) after 4 dummy scans. Inverse gated ^{13}C decoupling was used for samples containing ^{13}C-
253 Glucose to ensure the spectra were quantitative. The zgigpr sequence was used with ^{13}C
254 decoupling during ^{1}H acquisition (396 ms), a recycle delay of 10 s, and presaturation at 4.7
255 ppm for water suppression. Thirty-two scans were accumulated (8k data points with a spectral
256 width of 20 ppm). The spectra were processed using Topspin 3.1 (Bruker, Rheinstatten,
257 Germany). The reported results are the average values obtained from at least three biological
258 replicates.

259 **2.9 Calculation of Growth Rates and Extracellular Fluxes**

260 Growth rates and extracellular metabolite fluxes were determined from the time courses of
261 biomass, glucose, gluconate and 2-KG concentrations, as measured by NMR. All calculations
262 were performed using PhysioFit 1.0.2 (Peiro et al., 2019) https://github.com/MetaSys-
263 LISBP/PhysioFit)). MBPeGFP and mCherry production rates ($q_{MBPeGFP}$ and $q_{mcherry}$) were
264 calculated by multiplying the respective yields by the growth rate.

265 **2.10 ^{13}C-labeled samples and quantitative isotopic analysis.**

266 Samples of culture medium (100 µL) for quantitative isotopic analyses and ^{13}C-metabolic flux
267 analyses were collected during the first growth phase (between OD_{600} 2 and 4). The samples
268 were plunged and vigorously mixed in 2 mL of methanol/acetonitrile/H_2O (4:4:2) precooled at
269 -20 °C, incubated for 2 h at -20 °C, evaporated overnight in a SpeedVac (SC110A SpeedVac
270 Plus, ThermoSavant, Waltham, MA, USA) and stored at -80 °C until IC-MS analysis. The cell
271 extracts were then resuspended in 100 µL deionized water, and centrifuged at 14,500 *g* for 10
272 min at 4 °C to remove cell debris. Mass fractions of intracellular metabolites were quantified
273 using an ion chromatograph (IC; Thermo Scientific Dionex ICS- 50001 system; Dionex,
274 Sunnyvale, CA, United States) coupled to an LTQ Orbitrap mass spectrometer (Thermo Fisher

275 Scientific, Waltham, MA, United States) equipped with a heated electrospray ionization (HESI)
276 probe. Fourier transform mass spectra were recorded in full-scan negative ion mode at a
277 resolution of 60,000 at m/z = 400. The ion chromatography and mass spectrometry
278 experiments are described in greater detail elsewhere (Vogeleer and Létisse, 2022). In total,
279 three samples were analyzed for each of three independent biological replicates.

280 Isotopologues were quantified from 11 metabolic intermediates covering the central
281 metabolism (6-phosphogluconate, glucose 6-phosphate, fructose 6-phosphate, fructose 1,6-
282 bisphosphate, 2/3-phosphoglycerate, phosphoenolpyruvate, ribose 5-phosphate,
283 sedoheptulose 7-phosphate, citrate/isocitrate, malate and succinate). The mass fractions
284 were corrected for naturally occurring isotopes, using IsoCor 2.2.0 ((Millard et al., 2019),
285 https://github.com/MetaSys-LISBP/IsoCor) and high resolution spectra (60,000 at m/z = 400),
286 with corrections for the natural abundance and isotopic purity (99 %) of the tracer element.

287 **2.11 ^{13}C-Metabolic flux analyses**

288 ^{13}C metabolic fluxes were calculated using the software influx_s (Sokol et al., 2012), based on
289 a flux model that included the mass balances and carbon atom transitions of *P. putida*'s main
290 central metabolic pathways (Kohlstedt and Wittmann, 2019; Nikel et al., 2015): glucose
291 uptake, glycolysis (EMP), pentose phosphate pathway (PPP), ED pathway, tricarboxylic acid
292 cycle (TCA), anaplerotic reactions, and gluconate and 2-KG secretion. Following Kohlstedt and
293 Wittmann (2019), the flux through the Kdgk reaction was fixed at 4.9 % of the flux through the
294 Gntk reaction. Precursor requirements for biomass synthesis were estimated based on the
295 composition of the biomass (van Duuren et al., 2013) and growth rates. Similarly, precursor
296 requirements for the synthesis of heterologous protein were estimated from the protein
297 sequence and from protein production rates. Intracellular fluxes were estimated by fitting i)

298 extracellular fluxes (glucose uptake, and gluconate, 2-KG, biomass and protein production)
299 and ii) the ^{13}C-labelling patterns of intracellular metabolites measured by IC-MS. A chi-square
300 statistical test was used to assess the goodness-of-fit (based on 95 % confidence intervals) for
301 each condition. For comparison, the estimated fluxes were then normalized to the rate of
302 substrate uptake, set to 100. For each condition, the mean fluxes and the corresponding
303 standard deviations were determined from three independent biological replicates. The
304 isotopic data and metabolic fluxes for each independent biological replicate are given in Table
305 S2 in the supplementary material. All model files and flux calculation results are available at
306 https://github.com/MetaSys-LISBP/pseudomonas_metabolic_burden.

307 **2.12 Calculation of carbon, redox and energy balances**

308 The carbon balance was determined by calculating the proportion of carbon converted from
309 glucose to biomass, gluconate, 2-KG, CO_2 and heterologous protein during the exponential
310 phase as outlined in the results section. The amounts of biomass, gluconate, 2-KG and
311 heterologous protein produced were quantified as described above. The amount of CO_2
312 produced during the exponential phase was calculated from the percentage concentrations
313 of CO_2 and N_2 measured in the gas output using a Dycor ProLine Process mass spectrometer
314 (Ametek, Berwyn, PA, USA). The biomass formula was assumed to be $C_1H_{1.52}O_{0.41}N_{0.27}P_{0.02}S_{0.01}$
315 (van Duuren et al., 2013).

316 NADPH production and consumption fluxes were estimated by summing the fluxes through
317 all reactions producing or consuming NADPH along with NADPH fluxes for the synthesis of
318 biomass (anabolism) and heterologous protein. Similarly, ATP production *via* substrate-level
319 phosphorylation was calculated by summing the fluxes of ATP-producing reactions and
320 subtracting the fluxes of ATP-consuming reactions. ATP produced *via* oxidative

321 phosphorylation was inferred from the production rates of NADH, $FADH_2$ and $FMNH_2$,
322 assuming P/O ratios of of 1.875 for the conversion of NADH and $PQQH_2$ into ATP and a P/O
323 ratio of 1.0 for the conversion of $FADH_2$ (Nikel et al., 2015). ATP demand was calculated by
324 summing the requirements for anabolism, non-growth-associated maintenance (van Duuren
325 et al., 2013), and for the biosynthesis of the heterologous protein, assuming 5 ATP equivalents
326 per amino acid residue added (Garett and Grisham, 1999).

327 **3. Results**

328 **3.1 Characterization of the metabolic burden in *P. putida***

329 To characterize the physiological impact of the metabolic burden due to heterologous protein
330 production in *P. putida* KT2440, we introduced a fluorescent protein under the control of a
331 constitutive promoter into the *att* site in the chromosome as a proxy for the biosynthetic
332 capacity of *P. putida* cells. We chose the mCherry fluorescent protein controlled by the *lacIp*
333 promotor from the *E. coli lac*-operon, which is not regulated when isolated from its original
334 genomic environment. The amount of mCherry produced during heterologous protein
335 production was therefore taken to be representative of the availability of cellular resources
336 and served as a proxy for the biosynthetic capacity of the cells (Ceroni et al., 2015).

337 The eGFP labelled protein chosen to impose a metabolic burden was introduced into *P. putida*
338 KT2440 cells on a plasmid under the control of an inducible promoter (Figure 2A). The eGFP
339 domain was fused to the C-terminus of MBP, forming a 623-amino-acid fusion protein,
340 MBPeGFP (Figure 2B). The advantages of MBPeGFP for this study were that the fluorescence
341 emitted by eGFP could be used to estimate protein yields during growth, while the MBP
342 domain increased solubility and limited aggregation (Raran-Kurussi et al., 2015). To facilitate
343 purification, a His-tag was added to the C-terminal part of the eGFP domain (sequence is

344 available in supplementary data). The MBPeGFP encoding gene was integrated into
345 pSEVA438, under the control of a XylS/Pm expression system induced by 3-MB.

346 The associated metabolic burden was quantified in terms of the growth, biosynthetic capacity
347 and heterologous protein production of *P. putida* CAP (pSEVA438_MBPeGFP) cultures in
348 microtiter plates. The expression of MBPeGFP was modulated by exposing the cells to various
349 concentrations of 3-MB inducer, from 0 to 1000 µM (Figure 2C).

350 Four types of behavior can be distinguished in these data. First, at very low 3-MB
351 concentrations (< 0.5 µM), the small amounts of MBPeGFP produced did not represent a
352 metabolic burden since there was no impact on *P. putida* growth or biosynthetic capacity
353 (mCherry production). Note that some MBPeGFP production was observed even in the
354 absence of inducer, indicating that as reported previously (Balzer et al., 2013), the XylS/Pm
355 expression system is slightly leaky. The growth rate (μ_{max}) was 0.57 ± 0.02 h^{-1} , as reported in
356 the literature for this strain when grown on glucose (Kohlstedt and Wittmann, 2019; Kozaeva
357 et al., 2021). Second, exposure to between 0.5 and 10 µM 3-MB was associated with a
358 dramatic reduction in μ_{max} from 0.57 ± 0.02 h^{-1} to 0.15 ± 0.02 h^{-1}, and increased mCherry
359 production (Figure 2D). This relationship between growth rate and biosynthetic capacity is in
360 agreement with Ceroni et al.'s findings in *E. coli* (Ceroni et al., 2015). The MBPeGFP production
361 rate remained constant, meaning that the decrease in cell growth did not directly translate
362 into a higher heterologous protein production rate (Figure 2E). Under these conditions,
363 resource sharing is detrimental to cell growth with no clear benefit in terms of protein
364 production. From 10 to 250 µM 3-MB, the MBPeGFP production rate gradually increased while
365 cell growth and mCherry production remained constant. The MBPeGFP production rate at 250
366 µM 3-MB was twice what it was at 10 µM 3-MB. Here too, the rates of cell growth and protein

367 production did not directly counterbalance each other, indicating that the coordination of
368 these processes is more complex than a simple sharing of cellular resources. Finally, exposing
369 the cells to more than 250 µM 3-MB did not increase the MBPeGFP production rate and had
370 no additional impact on their growth rate or biosynthetic capacity.

371 Having observed that exposing *P. putida* CAP (pSEVA438_MBPeGFP) to various concentrations
372 of inducer generated different levels of metabolic burden, we explored how the central
373 metabolism of the host copes with *low* (without inducer), *medium* (10 µM 3-MB), and *high*
374 (1000 µM 3-MB) degrees of metabolic burden.

375 **3.2 Quantitative analysis of *P. putida* physiology during heterologous protein production.**

376 Cell cultures were scaled-up from micro-titer plates to bioreactors so that key environmental
377 parameters (pH, dissolved oxygen tension (DOT), temperature, agitation, *etc.*) could be
378 adjusted precisely. *P. putida* CAP (pSEVA438_MBPeGFP) was cultivated in minimal medium
379 supplemented with 10 $g \cdot L^{-1}$ glucose as sole carbon source and containing either none, 10 µM
380 or 1000 µM 3-MB. Figure 3 compares the resulting culture profiles with those obtained under
381 the same conditions with WT *P. putida* KT2440.

382 In the absence of inducer, *P. putida* CAP (pSEVA438_MBPeGFP) grew at the same rate (0.58 ±
383 0.03 h^{-1}) in the bioreactor as in the microtiter plate (Figure 2) and as the WT strain in the
384 bioreactor (Table1). This value is also similar to those reported in the literature for growth on
385 glucose (Kohlstedt and Wittmann, 2019). In the presence of 10 or 1000 µM 3-MB, the growth
386 rates in the exponential phase were half (0.29 ± 0.01 h^{-1}) or one third (0.19 ± 0.04 h^{-1}) of the
387 non-induced value, respectively. As observed in microtiter plates, the production rate of
388 mCherry also decreased, by a factor of 1.3 and 1.7, respectively.

389 Under non-induced conditions, MBPeGFP represented an estimated 0.39 ± 0.07 % of the total
390 CDW, confirming the slight leakiness of the XylS/Pm expression system. In the presence of 10
391 µM and 1000 µM inducer, the production rate of MBPeGFP increased by factors of 5 and
392 almost 12, respectively, leading to heterologous protein yields of 4.15 ± 0.28 % and 14.07 ±
393 0.90 % of the total CDW (Table 1).

394 These results show that the chosen induction conditions had the expected effects, namely a
395 *low* metabolic burden in the absence of induction, and *medium* and *high* burdens with 10 and
396 1000 µM 3-MB, respectively.

397 **3.3 Protein production strongly modifies the periplasmic metabolism**

398 The burden imposed by the synthetic expression system for maintenance and protein
399 production leads to profound modifications of the central metabolism (Wittmann et al., 2007).
400 To investigate the metabolic rearrangements occurring in *P. putida* in response to
401 heterologous protein production, the dynamic profiles of extracellular metabolites in the
402 culture media of WT and CAP (pSEVA438_MBPeGFP) *P. putida* strains were quantified by
403 NMR.

404 *P. putida* has been observed to produce gluconate and small amounts of 2-KG during
405 exponential growth on glucose, with concentrations peaking at 5 mM and 0.2 µM,
406 respectively, and both compounds subsequently being co-consumed with glucose (Nikel et al.,
407 2015). In the absence of inducer, a similar profile was observed here for gluconate, while the
408 2-KG concentration dropped below the limit of detection (Figure 3, upper panel). The
409 concentrations of both compounds reached much higher levels in the presence of inducer,
410 with the concentration of 2-KG peaking at 2 and 4 mM in the presence of 10 and 1000 µM 3-

411 MB, respectively. Note that no other metabolites were found to accumulate in these
412 experiments.

413 The rates of glucose consumption (q_{Glc}), gluconate and 2-KG production (q_{Gnt} and q_{2KG}), and
414 mCherry and MBPeGFP production ($q_{mcherry}$, q_{GFP}) were determined during the exponential
415 growth phase based on the concentrations of biomass and extracellular metabolites and on
416 protein fluorescence. The fact that these rates were constant throughout the exponential
417 growth phase indicates that the cells had reached a steady state (Figure 3, upper panel; Table
418 1 & Supplementary Figure S3). Under low MBPeGFP production conditions, the rates of
419 glucose consumption (6.9 $mmol \cdot g^{-1} \cdot h^{-1}$ ± 0.54) and gluconate production (0.8 ± 0.2 $mmol \cdot g^{-}$
420 $^{1} \cdot h^{-1}$) were similar to those calculated for the WT strain (Table 1) (Kohlstedt and Wittmann,
421 2019)), while the extracellular concentration of 2-KG was below the limit of detection. Under
422 medium and high MBPeGFP production conditions, glucose consumption decreased to 4.6 ±
423 0.4 $mmol \cdot g^{-1} \cdot h^{-1}$ in the presence of 10 µM 3-MB and 3.4 ± 0.3 $mmol \cdot g^{-1} \cdot h^{-1}$ at 1000 µM 3-MB,
424 while 2-KG production was 0.2 $mmol \cdot g^{-1} \cdot h^{-1}$ under both conditions (Table 1). CO_2 production
425 was also lower under these conditions than in the WT strain.

426 These results indicate that heterologous protein production caused a marked slowdown of
427 metabolic activity in *P. putida* CAP (pSEVA438_MBPeGFP), as reflected in particular by the
428 lower rate of glucose consumption. More surprising is the sharp change in periplasmic
429 metabolism evidenced by the accumulation of 2-KG. To the best of our knowledge, this
430 phenomenon has never previously been reported in *P. putid*a, but it is similar to the acetate
431 overaccumulation observed under recombinant protein production conditions in *E. coli* (San
432 et al., 1994; Ying Lin and Neubauer, 2000).

433 **3.4 Heterologous protein production consumes very little carbon but profoundly alters the**
434 **distribution of carbon usage in *P. putida***

435 The carbon balance was calculated for each condition by summing the amounts of carbon
436 used to produce biomass, gluconate, 2-KG, CO_2 and heterologous protein (Figure 3, lower
437 panel). These compounds accounted for nearly 100 % of carbon usage in each case (WT: 98.7
438 ± 2 %, uninduced: 99.0 ± 2 %, 10 µM: 98.2 ± 6 %, 1000 µM: 99.1 ± 8 %), confirming that no
439 other carbon molecules were produced in significant amounts. Under low MBPeGFP
440 production conditions, the proportions of carbon used for biomass, gluconate, CO_2 and 2-KG
441 production were similar to those observed for the WT strain. The proportion of carbon used
442 for biomass production decreased to 0.461 ± 0.006 Cmol/Cmol and 0.387 ± 0.069 Cmol/Cmol
443 under medium and high protein production conditions, respectively, while the proportion of
444 carbon diverted to gluconate decreased by a factor of 1.3 and 2.6, respectively, and the
445 fraction used for 2-KG production increased significantly to 5.2 ± 1.3 % of total carbon usage
446 at 10 µM 3-MB and 8.6 ± 4.0 % 1000 µM 3-MB. Remarkably, the total amount of carbon
447 converted into gluconate and 2-KG was constant across all studied conditions.

448 The proportion of carbon used for MBPeGFP production was negligible in the absence of
449 inducer, and was just 0.024 ± 0.015 Cmol/Cmol and 0.041 ± 0.010 Cmol/Cmol in the presence
450 of 10 and 1000 µM 3-MB, respectively. However, the amount of carbon excreted as CO_2 by
451 the cell increased from 0.325 ± 0.048 Cmol/Cmol without inducer to 0.372 ± 0.017 Cmol/Cmol
452 in the presence of 10 µM 3-MB and 0.440 ± 0.052 Cmol/Cmol with 1000 µM 3-MB (Figure 3,
453 lower panel). In other words, under conditions of significant heterologous protein production,
454 part of the carbon normally used for biomass was completely oxidized into CO_2. Therefore,

455 although production of the heterologous protein only accounted for a small percentage of the
456 total carbon consumed, it had a profound impact on cellular metabolism.

457 **3.5 Metabolic flux analyses reveal metabolic rearrangements in the central metabolism of**
458 ***P. putida***

459 We employed ^{13}C metabolic flux analysis to measure the alterations in the central metabolism
460 of *P. putida* in response to heterologous protein production. To minimize the impact of culture
461 history, we quantified ^{13}C incorporation in central metabolites that have a faster turnover rate
462 compared to the end products of the carbon metabolism.

463 **3.5.1 Metabolic flux map for *P. putida* WT**

464 We first compared the central metabolic flux distribution measured in WT *P. putida* KT2440
465 (Figure 4) with those based on LC- or GC-MS based ^{13}C metabolic flux analyses reported in the
466 literature (Nikel et al., 2015; Kohlstedt and Wittmann, 2019). Similarly to previous reports, we
467 found that glucose was mainly oxidized in the periplasm into gluconate (91 %) by glucose
468 dehydrogenase (Gcd) and to a lesser extent (5 %) into 2-KG by gluconate dehydrogenase
469 (Gad), with a significant (> 10 %) gluconate excretion into the culture supernatant. Most of the
470 gluconate (76 %) was phosphorylated into 6-phosphogluconate (6PG). At this metabolic node,
471 the carbon flux through the 2-KG bypass was 4 %. 6PG was mainly channeled into the ED
472 pathway *via* 2-keto-3-deoxy-6-phosphogluconate (2-KDPG), cleaved into glyceraldehyde-3-
473 phosphate (G3P) and pyruvate. G3P was mainly driven toward the low EMP pathway, where
474 it converged with 2-KDPG breakdown at the pyruvate node. Approximatively 20 % of G3P was
475 directed toward the EDEMP cycle. Despite this flux, glucose was mainly oxidated in the
476 periplasm, where the oxidative flux was 6 times higher than in the cytoplasm. The flux
477 channeled through the EDEMP cycle is however essential as it increases the NADPH reducing

478 power and ensures the supply of precursors (R5P, E4P, F6P) required for anabolism. Finally,
479 pyruvate was mainly driven toward the TCA cycle, with no significant flux through the
480 glyoxylate shunt. The concerted action of pyruvate dehydrogenase (Pdh) and pyruvate
481 carboxylase (Pyc) fuels the TCA cycle while replenishing the supply for anabolic needs. The flux
482 through malic enzyme (Mae) was remarkably high, contributing approximately one quarter of
483 the total influx into the pyruvate pool.

484 **3.5.2 Metabolic flux map for *P. putida* CAP (pSEVA438_MBPeGFP).**

485 Next, we examined the metabolic flux distributions in the central metabolism of *P. putida* CAP
486 (pSEVA438_MBPeGFP) under different degrees of metabolic burden.

487 As mentioned above, *P. putida* CAP (pSEVA438_MBPeGFP) produced small amounts of
488 heterologous protein even in the absence of inducer, exploiting only a part of its free capacity.
489 The flux distribution in the absence of inducer was similar to the one determined for the WT
490 strain (Figure 4B), indicating that using a small amount of *P. putida*'s free capacity only has a
491 negligible effect on the carbon flux distribution. In other words, this metabolic leeway can be
492 exploited to produce exogenous compounds such as proteins without affecting the cellular
493 machinery. Increasing this free capacity would therefore appear to be a viable strategy to
494 increase the amount of heterologous protein that can be produced without imposing a
495 metabolic burden. For example, removing 4.3 % of dispensable genes from *P. putida*'s genome
496 (including genes encoding for flagellar motility and genome stability) has been observed to
497 improve heterologous protein yields by 40 % (Lieder et al., 2015).

498 In contrast, the central metabolic flux distribution of *P. putida* CAP (pSEVA438_MBPeGFP) was
499 profoundly altered under medium and high metabolic burdens. First, periplasmic gluconate
500 oxidation into 2-KG by FAD-dependent Gad increased up to 2-fold without any significant

501 change either in gluconate oxidation through the ED pathway *via* gluconate kinase (GntK) or
502 *via* 2-KG bypass. The increased flux through Gad was compensated by a 2-fold decrease in
503 excreted gluconate and by significant excretion of 2-KG. Therefore this metabolic reshuffling
504 resulted mainly in increased production of $FADH_2$ through Gad flux.

505 Second, whereas the flux through the EDEMP cycle tended to decrease under increased
506 MBPeGFP production, the flux through the other pathways of the central metabolism
507 increased, particularly through the endergonic subset of the EMP pathway and in the TCA
508 cycle. The fluxes through phosphoglycerate kinase (Pgk), phosphopyruvate hydratase (Eno)
509 and pyruvate kinase (Pyk) increased by respectively 10 %, 12 % and 7 % under medium
510 MBPeGFP production compared with the low production condition, and by 22 %, 26 % and 50
511 % respectively at high MBPeGFP production. The fluxes through the TCA cycle dehydrogenases
512 (isocitrate dehydrogenase (Idh), α-ketoglutarate dehydrogenase (AkgdH), succinate
513 dehydrogenase (Sdh) and to a lesser extent malate dehydrogenase (Mdh)) increased by
514 roughly 15% and 25% under medium and high MBPeGFP production conditions relative to the
515 baseline level. Note that the glyoxylate cycle was not activated by protein production.

516 This analysis of metabolic fluxes shows that heterologous protein production leads to a
517 reshuffling of *P. putida*'s central carbon metabolism, with carbon fluxes redirected toward the
518 oxidative catabolic pathway. This presumably provides the extra chemical and redox energy
519 required to synthesize the heterologous protein and counter the corresponding stress while
520 still satisfying basic housekeeping needs.

521 **3.6 *P. putida* generates an apparent excess of ATP under heterologous protein production**
522 **conditions**

523 The rearrangement of central carbon fluxes for heterologous protein production point to an
524 important adjustment of energy metabolism. We therefore calculated redox and ATP fluxes
525 from the measured flux distributions as described in the Materials & Methods section.

526 In agreement with previous studies (Kohlstedt and Wittmann, 2019; Nikel et al., 2015), our
527 data indicate that *P. putida* WT generates a catabolic excess of NADPH (Figure 5A). Isocitrate
528 dehydrogenase (Idh) supplies roughly half of the NADPH, and malic enzyme a third. The
529 oxidative branch of the PP pathway contributes very little, despite it being the main
530 contributor to NADPH production in other microorganisms, such as *E. coli* (Nicolas et al.,
531 2007). The apparent surplus of NADPH is converted into NADH *via* transhydrogenase activities
532 (PntAB and SthA). As expected in aerobic growth, ATP is overwhelmingly produced by
533 oxidative phosphorylation, mainly for anabolic purposes (Figure 5B). Unlike NADPH, ATP-
534 production and consumption balance out (>93 %).

535 Compared to the WT strain, NADPH production fluxes were respectively 27 %, 45 % and 54 %
536 lower in the CAP (pSEVA438_MBPeGFP) strain under low, medium and high MBPeGFP
537 production conditions, respectively (Figure 5A). While the NADPH consumption flux was
538 similar to the WT strain's under low MBPeGFP production conditions, it was much lower under
539 medium and high MBPeGFP production. NADPH was mainly used for anabolism, and less than
540 one-fifth (8.6%) of the total NADPH consumed was used for heterologous protein synthesis
541 under high protein production conditions. As in the WT strain, NADPH production exceeded
542 the cellular demand, with the excess amount accounting for a large proportion of total NADPH
543 production under medium and high MBPeGFP production conditions (43 ± 11 % and 53 ± 5 %
544 respectively). Excessive NADPH production during heterologous protein production has also
545 been reported for other microorganisms (Daniels et al., 2018; Driouch et al., 2012; Nocon et

546 al., 2016; Toya et al., 2014). Similar to the WT strain, the apparent surplus of NADPH was
547 converted into NADH by transhydrogenase.

548 Regarding energy metabolism, low MBPeGFP production did not have an obvious impact on
549 production and consumption fluxes in the CAP (pSEVA438_MBPeGFP) strain (Figure 5B). In
550 contrast, under medium and high protein production conditions, ATP production and
551 consumption fluxes were reduced by 36 % and 39 %, respectively, compared to the WT strain,
552 while the contributions of oxidative phosphorylation and anabolic demand to the ATP balance
553 remained close to the levels estimated in the WT strain. Remarkably, the amount of ATP used
554 for heterologous protein production was very low, even under high induction. As observed for
555 NADPH, a large apparent surplus of ATP was generated upon medium and high MBPeGFP
556 production, representing respectively 25 % and 40 % of the total ATP consumed. This large
557 apparent excess probably covered unquantified energy usages in protein biosynthesis, such
558 as protein folding, as well as cellular adaptations to the stresses associated with protein
559 overproduction.

560 **3.7 Metabolic control analysis of heterologous protein production**

561 We then aimed to quantify the extent of control exerted by heterologous protein production
562 on metabolic fluxes using flux control coefficients (C_p^J), which quantify the degree of control
563 exerted by a given parameter *p,* here the protein production rate, on each flux *J*. Control
564 coefficients were calculated as the fractional change in the steady-state flux *J* in response to
565 a fractional change in *p* (Fell and Thomas, 1995; Heinrich and Rapoport, 1974; Kacser and
566 Burns, 1973):

567 $$C_p^J = \frac{\delta J}{J} \Big/ \frac{\delta p}{p} = \frac{\delta \ln J}{\delta \ln p}$$

568 If the C_p^J coefficients remain constant across different experiments in which *p* is modulated,
569 their value can be estimated by fitting a linear function to a *ln-ln* plot, whose slope is equal to
570 the control strength. Here, we used (steady-state) data collected for the various levels of
571 protein production (Figure 4 & supplemental Table S2) to estimate the control exerted by
572 protein production on carbon and energy fluxes. Note that the C_p^J coefficients measure the
573 sensitivity of the system to both direct metabolic regulation (though thermodynamics and
574 metabolite-enzyme interactions), as well as to the indirect (hierarchical) action of signal
575 transduction and gene expression.

576 The degree of control exerted by the MBPeGFP production rate on carbon and energy fluxes
577 was investigated at the level of individual reactions and for more global processes such as
578 growth and ATP and NADPH formation. This analysis provided an overall picture of the cellular
579 processes affected by heterologous protein production (Figure 6). Among the analyzed fluxes,
580 a majority of fluxes (25 out of 40, accounting for 63 %) showed a significant correlation with
581 protein production ($r^2 > 0.5$, $p < 0.02$). This indicates that the control exerted on these
582 reactions remained stable across all MBPeGFP production conditions. The low r^2 values (high
583 p-values) obtained for the other fluxes may indicate an absence of control (*e.g.* Gnd) or reflect
584 more complex, nonlinear control patterns that cannot be captured by linear regression (*e.g.*
585 Ppc) (Figure S4).

586 Looking more closely at the control coefficients, MBPeGFP production exerted a negative
587 control on virtually all fluxes (with coefficients ranging from -0.17 to -0.99), in line with the
588 global decrease in fluxes observed in response to MBPeGFP production. This negative control
589 was observed for glucose uptake (-0.30±0.05, $r^2 = 0.80$, $p = 5.10^{-4}$), periplasmic glucose
590 oxidation (C_p^{gcd} = -0.59±0.10, $r^2 = 0.80$, $p = 5.10^{-4}$), the ED pathway (C_p^{edd} = -0.62±0.11, r^2 =

591 0.79, p = 6.10^{-4}), the EMP pathway (C_p^{pgk} = -0.52±0.09, r^2 = 0.80, p = 5.10^{-4}), and the TCA cycle

592 (C_p^{cs} = -0.53±0.09, r^2 = 0.83, p = 3.10^{-4}). Significant control was also observed on ATP fluxes

593 ($C_p^{ATP_prod}$ = -0.20±0.04, r^2 = 0.78, p = 8.10^{-4}), with similar levels of control on ATP production

594 *via* oxidative phosphorylation and *via* substrate phosphorylation, and on NADPH fluxes

595 ($C_p^{NADPH_prod}$ = -0.17±0.06, r^2 = 0.51, p = 0.02). The control on energy and redox fluxes was

596 weaker (coefficients between -0.17 and -0.19) than on carbon fluxes (coefficients between -

597 0.30 and -0.99), indicating that in *P. putida* CAP (pSEVA438_MBPeGFP), energy fluxes are less

598 sensitive to heterologous protein production than carbon fluxes are. These results also

599 indicate that the fraction of glucose used for energy production increased with the level of

600 heterologous protein production. These metabolic rearrangements were reflected in terms of

601 cell physiology by a strong control on the growth rate (C_p^{growth}= -0.46±0.08; r^2 = 0.79, p = 5.10^{-}

602 ^{4}).

603 These results offer a quantitative understanding of the impact of heterologous protein

604 production on *P. putida*'s metabolism. The level of control remained largely stable across the

605 three induction levels studied, indicating that all pathways responded smoothly to

606 heterologous protein production. The fact that the response of carbon fluxes was more

607 pronounced compared to energy fluxes highlights the flexibility of the central carbon

608 metabolism and the robustness of the energy metabolism in *P. putida*.

609 **Conclusions**

610 In this study, we conducted a detailed quantitative analysis to examine how *P. putida* responds

611 to different degrees of metabolic burden caused by heterologous protein production. Our

612 results indicate that low levels of heterologous protein production do not require any

613 metabolic adaptation, because the extra demand does not exceed *P. putida*'s free capacity.

614 However, when this free capacity is exceeded, growth is progressively inhibited and a global
615 slowdown of metabolism is observed. Despite the relatively low (< 5%) carbon usage
616 associated with heterologous protein production, our study revealed significant
617 rearrangements in metabolic fluxes. These rearrangements indicate that even a small fraction
618 of carbon dedicated to protein production can have a profound impact on the overall
619 metabolic network of *P. putida.* As revealed by metabolic control analysis, heterologous
620 protein production exerts a tighter control on carbon fluxes than on energy fluxes, suggesting
621 that the flexible nature of *P. putida*'s central metabolic network is solicited to maintain energy
622 production. The metabolic flux response indicates a smooth, progressive decoupling of
623 anabolism from catabolism, with energy production increasing far beyond the expected
624 energy demands for protein biosynthesis. Similar behaviour was observed in other micro-
625 organisms (Daniels et al., 2018; Driouch et al., 2012; Nocon et al., 2016; Toya et al., 2014),
626 highlighting the genericity of microbial response to metabolic burdens. The apparent excess
627 energy is presumably used for the transcription, translation and folding of the heterologous
628 protein and in processes associated with plasmid maintenance, expression and amplification.
629 Energy requirements for these different processes are difficult to quantify and appear to be
630 largely underestimated. Moreover, some of this surplus must also be used by the cells to
631 overcome the stresses caused by heterologous protein production. These stresses remain to
632 be elucidated and merit further investigation; indeed, a comprehensive understanding of the
633 stress imposed by heterologous protein production would help identify promising targets and
634 optimize and upscale production processes.

5. Conflict of Interest

The authors declare that the research was conducted in the absence of any commercial or financial relationships that could be construed as a potential conflict of interest.

6. Funding

This work was supported by the Agence Nationale de la Recherche [grant number ANR-18-CE92-0027-01] and the Deutsche Forschungsgemeinschaft (DFG) [Project number 406709163].

7. Acknowledgments

The authors thank MetaToul (Metabolomics & Fluxomics Facilities, Toulouse, France, www.metatoul.fr) and its staff for technical support and access to the NMR facility. MetaToul is part of the French National Infrastructure for Metabolomics and Fluxomics (www.metabohub.fr), funded by the ANR (MetaboHUB-ANR-11-INBS-0010). Edern Cahoreau is gratefully acknowledged for assistance with NMR spectroscopy. The French National Research Agency (ANR) and the German Research Foundation (DFG) are acknowledged for funding of the CHEAP project and the ANR for funding a post-doctoral fellowship to P.V.

8. References

Balzer, S., Kucharova, V., Megerle, J., Lale, R., Brautaset, T., Valla, S., 2013. A comparative analysis of the properties of regulated promoter systems commonly used for recombinant gene expression in Escherichia coli. Microbial Cell Factories 12, 26. https://doi.org/10.1186/1475-2859-12-26

Borkowski, O., Ceroni, F., Stan, G.-B., Ellis, T., 2016. Overloaded and stressed: whole-cell considerations for bacterial synthetic biology. Current Opinion in Microbiology, Antimicrobials. Microbial systems biology 33, 123–130. https://doi.org/10.1016/j.mib.2016.07.009

660 Ceroni, F., Algar, R., Stan, G.-B., Ellis, T., 2015. Quantifying cellular capacity identifies gene
661 expression designs with reduced burden. Nat Methods 12, 415–418.
662 https://doi.org/10.1038/nmeth.3339
663 Choi, K.-H., Schweizer, H.P., 2006. mini-Tn7 insertion in bacteria with single attTn7 sites:
664 example Pseudomonas aeruginosa. Nat Protoc 1, 153–161.
665 https://doi.org/10.1038/nprot.2006.24
666 Chung, C.T., Niemela, S.L., Miller, R.H., 1989. One-step preparation of competent Escherichia
667 coli: transformation and storage of bacterial cells in the same solution. Proc Natl Acad
668 Sci U S A 86, 2172–2175. https://doi.org/10.1073/pnas.86.7.2172
669 Daniels, W., Bouvin, J., Busche, T., Rückert, C., Simoens, K., Karamanou, S., Van Mellaert, L.,
670 Friðjónsson, Ó.H., Nicolai, B., Economou, A., Kalinowski, J., Anné, J., Bernaerts, K.,
671 2018. Transcriptomic and fluxomic changes in Streptomyces lividans producing
672 heterologous protein. Microb Cell Fact 17, 198. https://doi.org/10.1186/s12934-018-
673 1040-6
674 de Lorenzo, V., 2008. Systems biology approaches to bioremediation. Current Opinion in
675 Biotechnology, Chemical biotechnology / Pharmaceutical biotechnology 19, 579–589.
676 https://doi.org/10.1016/j.copbio.2008.10.004
677 de Lorenzo, V., Timmis, K.N., 1994. Analysis and construction of stable phenotypes in gram-
678 negative bacteria with Tn5- and Tn10-derived minitransposons. Methods Enzymol 235,
679 386–405. https://doi.org/10.1016/0076-6879(94)35157-0
680 del Castillo, T., Ramos, J.L., Rodríguez-Herva, J.J., Fuhrer, T., Sauer, U., Duque, E., 2007.
681 Convergent Peripheral Pathways Catalyze Initial Glucose Catabolism in Pseudomonas
682 putida: Genomic and Flux Analysis. J. Bacteriol. 189, 5142.
683 https://doi.org/10.1128/JB.00203-07
684 Driouch, H., Melzer, G., Wittmann, C., 2012. Integration of in vivo and in silico metabolic fluxes
685 for improvement of recombinant protein production. Metab Eng 14, 47–58.
686 https://doi.org/10.1016/j.ymben.2011.11.002
687 Fell, D.A., Thomas, S., 1995. Physiological control of metabolic flux: the requirement for
688 multisite modulation. Biochem J 311 (Pt1), 35–39. https://doi.org/10.1042/bj3110035
689 Garett, H.R., Grisham, M., Charles, 1999. Biochemistry, 2nd edition. ed. Sanders College
690 Publication, Fort Worth.
691 Heinrich, R., Rapoport, T.A., 1974. A linear steady-state treatment of enzymatic chains.
692 General properties, control and effector strength. Eur J Biochem 42, 89–95.
693 https://doi.org/10.1111/j.1432-1033.1974.tb03318.x
694 Kacser, H., Burns, J.A., 1973. The control of flux. Symp Soc Exp Biol 27, 65–104.
695 Kim, J., Park, W., 2014. Oxidative stress response in Pseudomonas putida. Appl Microbiol
696 Biotechnol 98, 6933–6946. https://doi.org/10.1007/s00253-014-5883-4
697 Kohlstedt, M., Wittmann, C., 2019. GC-MS-based 13C metabolic flux analysis resolves the
698 parallel and cyclic glucose metabolism of Pseudomonas putida KT2440 and
699 Pseudomonas aeruginosa PAO1. Metab Eng 54, 35–53.
700 https://doi.org/10.1016/j.ymben.2019.01.008
701 Kozaeva, E., Volkova, S., Matos, M.R.A., Mezzina, M.P., Wulff, T., Volke, D.C., Nielsen, L.K.,
702 Nikel, P.I., 2021. Model-guided dynamic control of essential metabolic nodes boosts
703 acetyl-coenzyme A–dependent bioproduction in rewired Pseudomonas putida.
704 Metabolic Engineering 67, 373–386. https://doi.org/10.1016/j.ymben.2021.07.014

705 Lichten, C.A., White, R., Clark, I.B., Swain, P.S., 2014. Unmixing of fluorescence spectra to
706 resolve quantitative time-series measurements of gene expression in plate readers.
707 BMC Biotechnology 14, 11. https://doi.org/10.1186/1472-6750-14-11
708 Lieder, S., Nikel, P.I., de Lorenzo, V., Takors, R., 2015. Genome reduction boosts heterologous
709 gene expression in Pseudomonas putida. Microb Cell Fact 14.
710 https://doi.org/10.1186/s12934-015-0207-7
711 Loeschcke, A., Thies, S., 2015. Pseudomonas putida—a versatile host for the production of
712 natural products. Appl Microbiol Biotechnol 99, 6197–6214.
713 https://doi.org/10.1007/s00253-015-6745-4
714 Millard, P., Delépine, B., Guionnet, M., Heuillet, M., Bellvert, F., Létisse, F., 2019. IsoCor:
715 isotope correction for high-resolution MS labeling experiments. Bioinformatics 35,
716 4484–4487. https://doi.org/10.1093/bioinformatics/btz209
717 Nicolas, C., Kiefer, P., Letisse, F., Krömer, J., Massou, S., Soucaille, P., Wittmann, C., Lindley,
718 N.D., Portais, J.-C., 2007. Response of the central metabolism of Escherichia coli to
719 modified expression of the gene encoding the glucose-6-phosphate dehydrogenase.
720 FEBS Lett 581, 3771–3776. https://doi.org/10.1016/j.febslet.2007.06.066
721 Nikel, P.I., Chavarría, M., Fuhrer, T., Sauer, U., de Lorenzo, V., 2015. Pseudomonas putida
722 KT2440 Strain Metabolizes Glucose through a Cycle Formed by Enzymes of the Entner-
723 Doudoroff, Embden-Meyerhof-Parnas, and Pentose Phosphate Pathways. J Biol Chem
724 290, 25920–25932. https://doi.org/10.1074/jbc.M115.687749
725 Nikel, P.I., de Lorenzo, V., 2018. Pseudomonas putida as a functional chassis for industrial
726 biocatalysis: From native biochemistry to trans-metabolism. Metabolic Engineering,
727 Metabolic Engineering Host Organism Special Issue 50, 142–155.
728 https://doi.org/10.1016/j.ymben.2018.05.005
729 Nikel, P.I., Martínez-García, E., de Lorenzo, V., 2014. Biotechnological domestication of
730 pseudomonads using synthetic biology. Nat Rev Microbiol 12, 368–379.
731 https://doi.org/10.1038/nrmicro3253
732 Nocon, J., Steiger, M., Mairinger, T., Hohlweg, J., Rußmayer, H., Hann, S., Gasser, B.,
733 Mattanovich, D., 2016. Increasing pentose phosphate pathway flux enhances
734 recombinant protein production in Pichia pastoris. Appl Microbiol Biotechnol 100,
735 5955–5963. https://doi.org/10.1007/s00253-016-7363-5
736 Oehler, S., 2009. Feedback Regulation of Lac Repressor Expression in Escherichia coli. J
737 Bacteriol 191, 5301–5303. https://doi.org/10.1128/JB.00427-09
738 Peiro, C., Millard, P., de Simone, A., Cahoreau, E., Peyriga, L., Enjalbert, B., Heux, S., 2019.
739 Chemical and Metabolic Controls on Dihydroxyacetone Metabolism Lead to
740 Suboptimal Growth of Escherichia coli. Appl Environ Microbiol 85, e00768-19.
741 https://doi.org/10.1128/AEM.00768-19
742 Poblete-Castro, I., Borrero-de Acuña, J.M., Nikel, P.I., Kohlstedt, M., Wittmann, C., 2017. Host
743 Organism: Pseudomonas putida, in: Industrial Biotechnology. John Wiley & Sons, Ltd,
744 pp. 299–326. https://doi.org/10.1002/9783527807796.ch8
745 Raran-Kurussi, S., Keefe, K., Waugh, D.S., 2015. Positional effects of fusion partners on the
746 yield and solubility of MBP fusion proteins. Protein Expr Purif 110, 159–164.
747 https://doi.org/10.1016/j.pep.2015.03.004
748 San, K.Y., Bennett, G.N., Aristidou, A.A., Chou, C.H., 1994. Strategies in high-level expression
749 of recombinant protein in Escherichia coli. Ann N Y Acad Sci 721, 257–267.
750 https://doi.org/10.1111/j.1749-6632.1994.tb47399.x

Sokol, S., Millard, P., Portais, J.-C., 2012. influx_s: increasing numerical stability and precision for metabolic flux analysis in isotope labelling experiments. Bioinformatics 28, 687–693. https://doi.org/10.1093/bioinformatics/btr716

Toya, Y., Hirasawa, T., Morimoto, T., Masuda, K., Kageyama, Y., Ozaki, K., Ogasawara, N., Shimizu, H., 2014. 13C-metabolic flux analysis in heterologous cellulase production by Bacillus subtilis genome-reduced strain. Journal of Biotechnology 179, 42–49. https://doi.org/10.1016/j.jbiotec.2014.03.025

Udaondo, Z., Molina, L., Segura, A., Duque, E., Ramos, J.L., 2016. Analysis of the core genome and pangenome of Pseudomonas putida. Environ Microbiol 18, 3268–3283. https://doi.org/10.1111/1462-2920.13015

van Duuren, J.B., Puchałka, J., Mars, A.E., Bücker, R., Eggink, G., Wittmann, C., dos Santos, V.A.M., 2013. Reconciling in vivo and in silico key biological parameters of Pseudomonas putidaKT2440 during growth on glucose under carbon-limited condition. BMC Biotechnology 13, 93. https://doi.org/10.1186/1472-6750-13-93

van Winden, W., Verheijen, P., Heijnen, S., 2001. Possible Pitfalls of Flux Calculations Based on 13C-Labeling. Metabolic Engineering 3, 151–162. https://doi.org/10.1006/mben.2000.0174

Vicente, M., Cánovas, J.L., 1973. Glucolysis in Pseudomonas putida: Physiological Role of Alternative Routes from the Analysis of Defective Mutants. J Bacteriol 116, 908–914. https://doi.org/10.1128/jb.116.2.908-914.1973

Vogeleer, P., Létisse, F., 2022. Dynamic Metabolic Response to (p)ppGpp Accumulation in Pseudomonas putida. Front Microbiol 13, 872749. https://doi.org/10.3389/fmicb.2022.872749

Volke, D.C., Calero, P., Nikel, P.I., 2020. Pseudomonas putida. Trends in Microbiology 28, 512–513. https://doi.org/10.1016/j.tim.2020.02.015

Wittmann, C., Weber, J., Betiku, E., Kromer, J., Bohm, D., Rinas, U., 2007. Response of fluxome and metabolome to temperature-induced recombinant protein synthesis in Escherichia coli. J Biotechnol 132, 375–84. https://doi.org/10.1016/j.jbiotec.2007.07.495

Ying Lin, H., Neubauer, P., 2000. Influence of controlled glucose oscillations on a fed-batch process of recombinant Escherichia coli. Journal of Biotechnology 79, 27–37. https://doi.org/10.1016/S0168-1656(00)00217-0

Zobel, S., Benedetti, I., Eisenbach, L., de Lorenzo, V., Wierckx, N., Blank, L.M., 2015. Tn7-Based Device for Calibrated Heterologous Gene Expression in Pseudomonas putida. ACS Synth. Biol. 4, 1341–1351. https://doi.org/10.1021/acssynbio.5b00058

787 **10. Table**

788 **Table 1**: **Growth parameters of glucose-grown *P. putida* KT2440 WT and *P. putida* CAP**
789 **(pSEVA438_MBPeGFP) for different inducer concentrations.** [a] Not detected. n=3

790 **9. Figures**

791 **Fig 1. Metabolic pathway of *P. putida* KT2440's central metabolism**. The EDEMP pathway is
792 circled in turquoise and the TCA cycle in water-green. Biomass precursors are indicated by
793 grey triangles. Arrow sizes reflect the intracellular carbon flux of glucose-grown cells relative
794 to the glucose uptake rate (set to 100 %) determined by Kohlstedt and Wittmann (Kohlstedt
795 and Wittmann, 2019). EII and EIII represent the C_2 and C_3 fragment pools, respectively, bound
796 to transketolase and transaldolase, and transferred to an aldose acceptor as described by
797 Kleijn et al. (2005). Reaction names and equations are provided in the supplemental data
798 (Supp data table S1).

799

800 **Fig. 2. Physiological response of *P. putida* CAP (pSEVA438_MBPeGFP) to heterologous**
801 **protein production.** Schematic representation of the engineered *P. putida* strain with a red
802 fluorescent protein gene (*mCherry*) integrated into the chromosome to monitor biosynthetic
803 capacity and the green fluorescent fusion protein MBPeGFP encoded on a
804 pSEVA438_*MBPeGFP* plasmid (A). Schematic representation of the MBPeGFP fusion protein
805 with an N-terminal maltose binding protein (MBP) domain, the eGFP domain and a C-terminal
806 His-tag sequence (B). Growth rate (C), mCherry production rate (D) and MBPeGFP production
807 rate (E) of *P. putida* CAP (pSEVA438_MBPeGFP) cultivated with different inducer

808 concentrations. Results are averages from at least 3 biological replicates. 3-MB: 3-methyl-
809 benzoate.

810

811 **Fig. 3: Growth profiles and carbon balance of glucose-grown *P. putida* KT2440 WT (A, E) and**
812 ***P. putida* CAP (pSEVA438_MBPeGFP) under low (B, F), medium (C, G) and high (D, H)**
813 **heterologous protein production conditions.** The first phase, during which samples were
814 collected and growth parameters were calculated, is highlighted in blue. The solid lines
815 represent the best fits obtained with physiofit (Peiro et al., 2019). The corresponding results
816 for the biological replicates are shown in Figure S2.

817

818 **Fig. 4 Relative carbon flux distributions of KT2440 WT (A) and *P. putida* CAP**
819 **(pSEVA438_MBPeGFP) (B) grown on glucose with or without 3-MB.** All flux values are
820 normalized to the specific glucose uptake rate of each condition, which was set to 100. Values
821 represent the mean ± standard deviation of two biological replicates for the WT strain (A) and
822 at least 3 biological replicates for the CAP (pSEVA438_MBPeGFP) strain (B). In panel B, the flux
823 values correspond from top to bottom to: low (without inducer), medium (10 µM 3-MB), and
824 high (1000 µM 3-MB) heterologous protein production conditions. Reaction names and
825 equations are provided in the supplemental data (Supp data table S1).

826

827 **Fig. 5. Redox and energy fluxes of *P. putida* KT2440 WT and *P. putida* CAP**
828 **(pSEVA438_MBPeGFP) grown on glucose with or without 3-MB.** The absolute fluxes
829 ($mmol \cdot g_{CDW}^{-1} \cdot h^{-1}$) related to the production and consumption of NADPH (A) and ATP (B) were
830 determined from the carbon fluxes shown in Figure 4. Results are averages from 2 biological

831 replicates for the WT strain and at least 3 biological replicates for the CAP
832 (pSEVA438_MBPeGFP) strain; error bars represent standard deviations. Abbreviations: Gnd:
833 6-phosphogluconate dehydrogenase; Zwf: Glucose-6-P 1-dehydrogenase; Mae: malic enzyme;
834 Idh: isocitrate deshydrogenase; Pgk: phosphoglycerate kinase; Pyk: pyruvate kinase; SucACD:
835 succinyl CoA synthetase; Ox-P: oxidative phosphorylation; 2-KG bypass: 2-ketogluconate
836 bypass; Ppc: phosphoenolpyruvate carboxylase; Pyc: pyruvate carboxylase; Gntk: gluconate
837 kinase; Glk: Glucokinase.

838

839

840 **Fig. 6. Control exerted on *P. putida*'s carbon and energy metabolism by heterologous protein**
841 **production.** Overview of the flux control coefficients (A). Control coefficients determined for
842 carbon and energy fluxes through the main pathways (glucose uptake, EMPP, EDP, TCA cycle,
843 ATP and NADPH production, and growth) (B), where dots represent experimental flux values
844 (expressed on a logarithmic scale), lines represent the best linear fits, and shaded areas
845 correspond to 95 % confidence intervals on the fits. Coefficients that could not be determined
846 reliably for some reactions are marked *n.d.*

Parameter	WT strain	*P. putida* CAP (pSEVA438-MBPeGFP)		
3-methyl-benzoate (µM)	0	0	10 µM	1000 µM
μ_{max} [(h^{-1})]	0.58 ± 0.02	0.58 ± 0.03	0.29 ± 0.01	0.19 ± 0.04
$q_{mcherry}$ (RLU · [g_{CDW} · h]$^{-1}$)	ND[a]	1120 ± 48	835 ± 81	659 ± 77
$q_{MBPeGFP}$ (mg · [g_{CDW} · h]$^{-1}$)	ND[a]	2.3 ± 0.5	9.3 ± 0.8	26.7 ± 6.0
q_{CO2} (mmol · [g_{CDW} · h]$^{-1}$)	13.0 ± 1.9	12.5 ± 1.9	10.7 ± 1.0	9.0 ± 1.3
$Y_{X/S}$ (g_X · mol^{-1})	82.1 ± 6.8	84.4 ± 4.2	66.5 ± 6.0	55.0 ± 7.0
$Y_{MBPeGFP}$ (mg · g_{CDW})	ND[a]	3.9 ± 0.7	41.5 ± 2.8	140.7 ± 9.0
q_{Glc} (mmol · [g_{CDW} · h]$^{-1}$)	7.0 ± 0.3	6.9 ± 0.5	4.6 ± 0.4	3.4 ± 0.3
q_{Gnt} (mmol · [g_{CDW} · h]$^{-1}$)	0.78 ± 0.22	0.81 ± 0.18	0.44 ± 0.04	0.15 ± 0.07
$q_{2\text{-}KG}$ (mmol · [g_{CDW} · h]$^{-1}$)	0.06 ± 0.01	0.01 ± 0.01	0.19 ± 0.05	0.22 ± 0.02

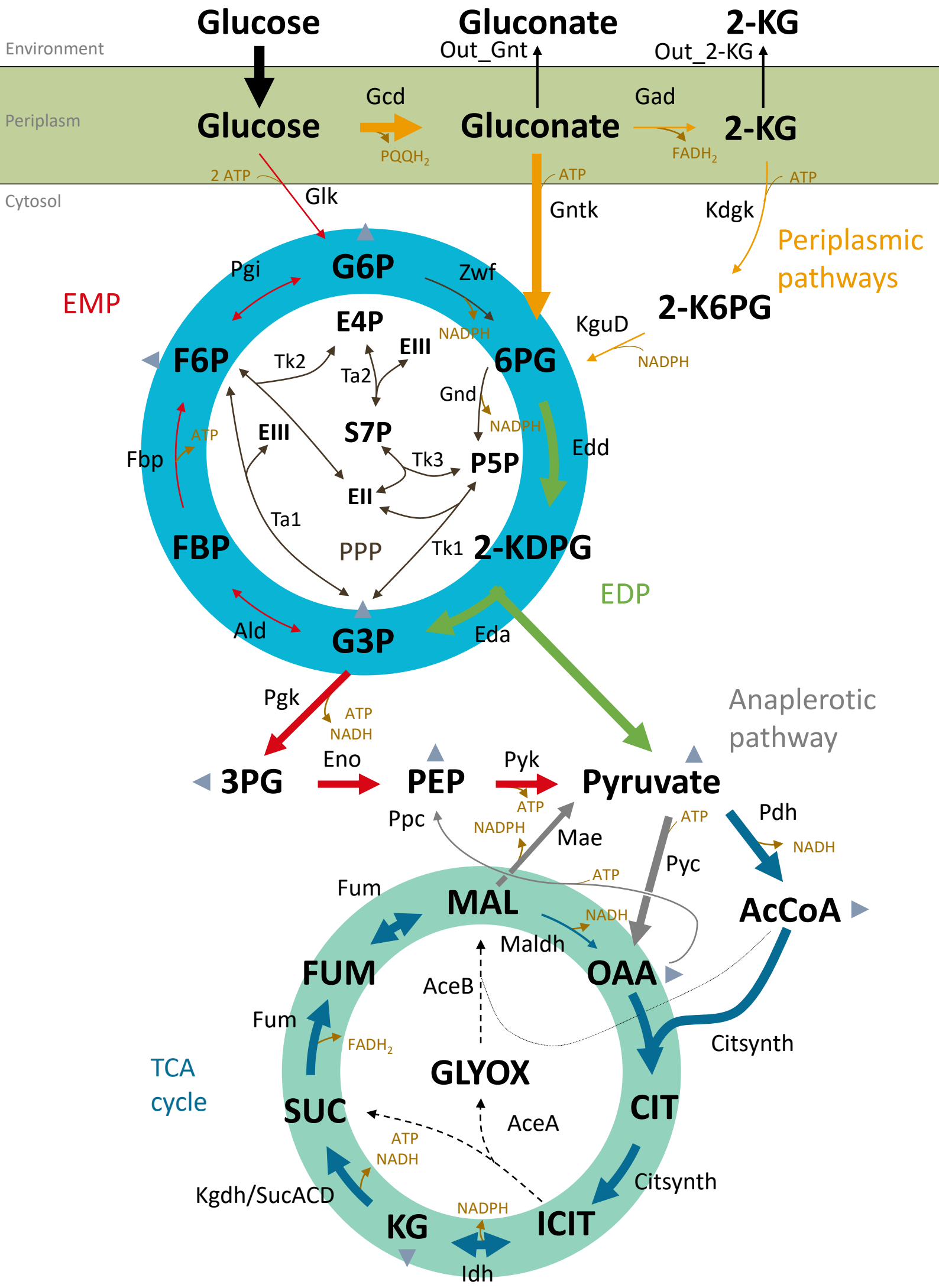
Environment
Periplasm
Cytosol
Glucose
Gluconate
2-KG
Out_Gnt
Out_2-KG
Glucose
Gcd
PQQH2
Gluconate
Gad
FADH2
2-KG
2 ATP
Glk
ATP
Gntk
ATP
Kdgk
Periplasmic pathways
2-K6PG
KguD
NADPH
EMP
G6P
Pgi
Zwf
NADPH
E4P
EIII
F6P
Tk2
Ta2
6PG
Gnd
NADPH
EIII
S7P
ATP
Fbp
Tk3
P5P
Edd
EII
Ta1
FBP
PPP
Tk1
2-KDPG
EDP
Ald
G3P
Eda
Pgk
ATP
NADH
Anaplerotic pathway
3PG
Eno
PEP
Pyk
Pyruvate
ATP
Ppc
NADPH
Mae
ATP
Pyc
Pdh
NADH
ATP
Fum
MAL
NADH
AcCoA
Maldh
FUM
OAA
AceB
Fum
FADH2
Citsynth
TCA cycle
GLYOX
SUC
CIT
AceA
ATP
NADH
Citsynth
Kgdh/SucACD
NADPH
KG
ICIT
Idh

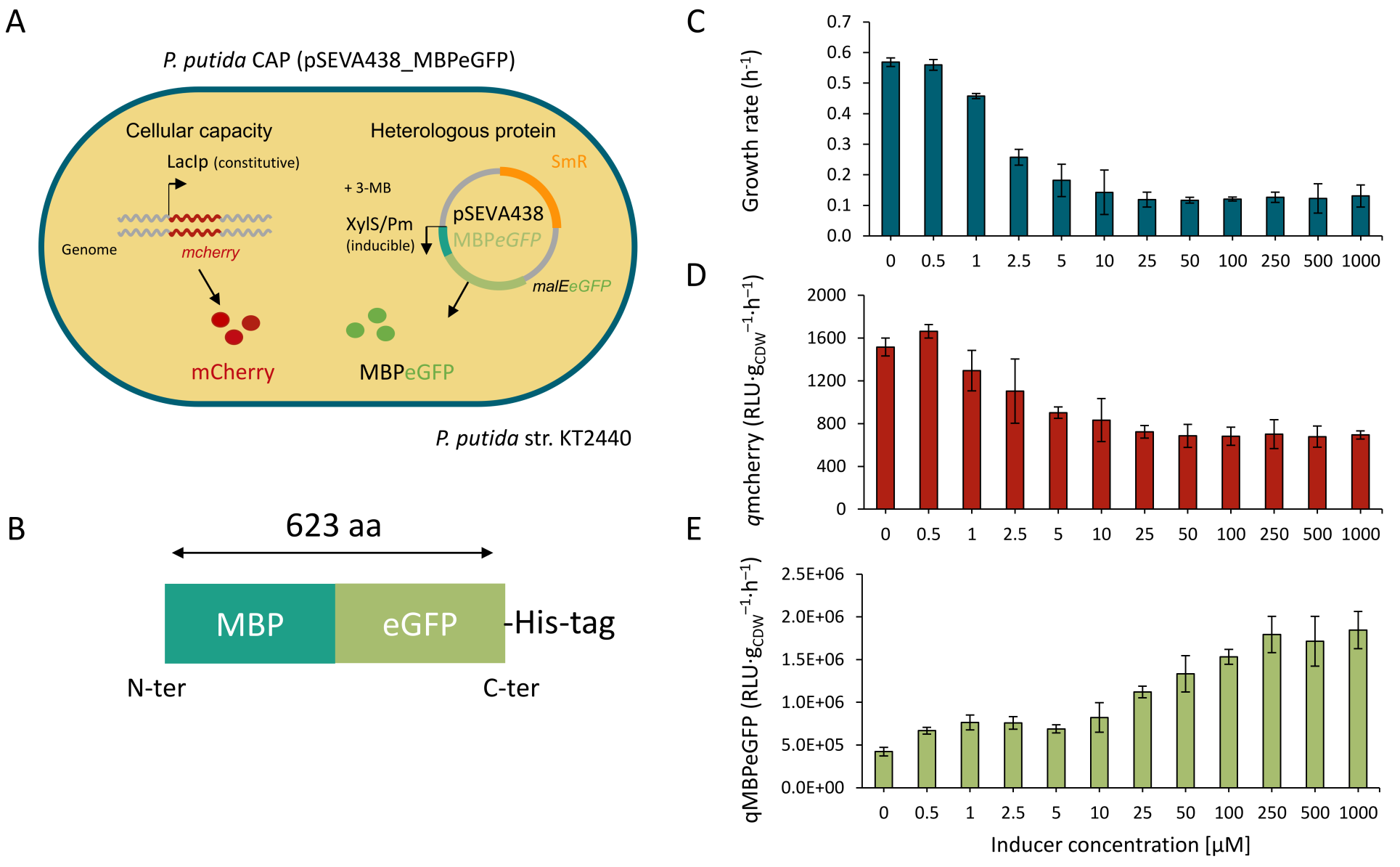
A
P. putida CAP (pSEVA438_MBPeGFP)
Cellular capacity
Heterologous protein
LacIp (constitutive)
SmR
+ 3-MB
pSEVA438
XylS/Pm
(inducible)
MBPeGFP
Genome
mcherry
malEeGFP
mCherry
MBPeGFP
P. putida str. KT2440
B
623 aa
MBP
eGFP
-His-tag
N-ter
C-ter
C
Growth rate (h-1)
0.7
0.6
0.5
0.4
0.3
0.2
0.1
0.0
0 0.5 1 2.5 5 10 25 50 100 250 500 1000
D
qmcherry (RLU·gCDW-1·h-1)
2000
1600
1200
800
400
0
0 0.5 1 2.5 5 10 25 50 100 250 500 1000
E
qMBPeGFP (RLU·gCDW-1·h-1)
2.5E+06
2.0E+06
1.5E+06
1.0E+06
5.0E+05
0.0E+00
0 0.5 1 2.5 5 10 25 50 100 250 500 1000
Inducer concentration [µM]

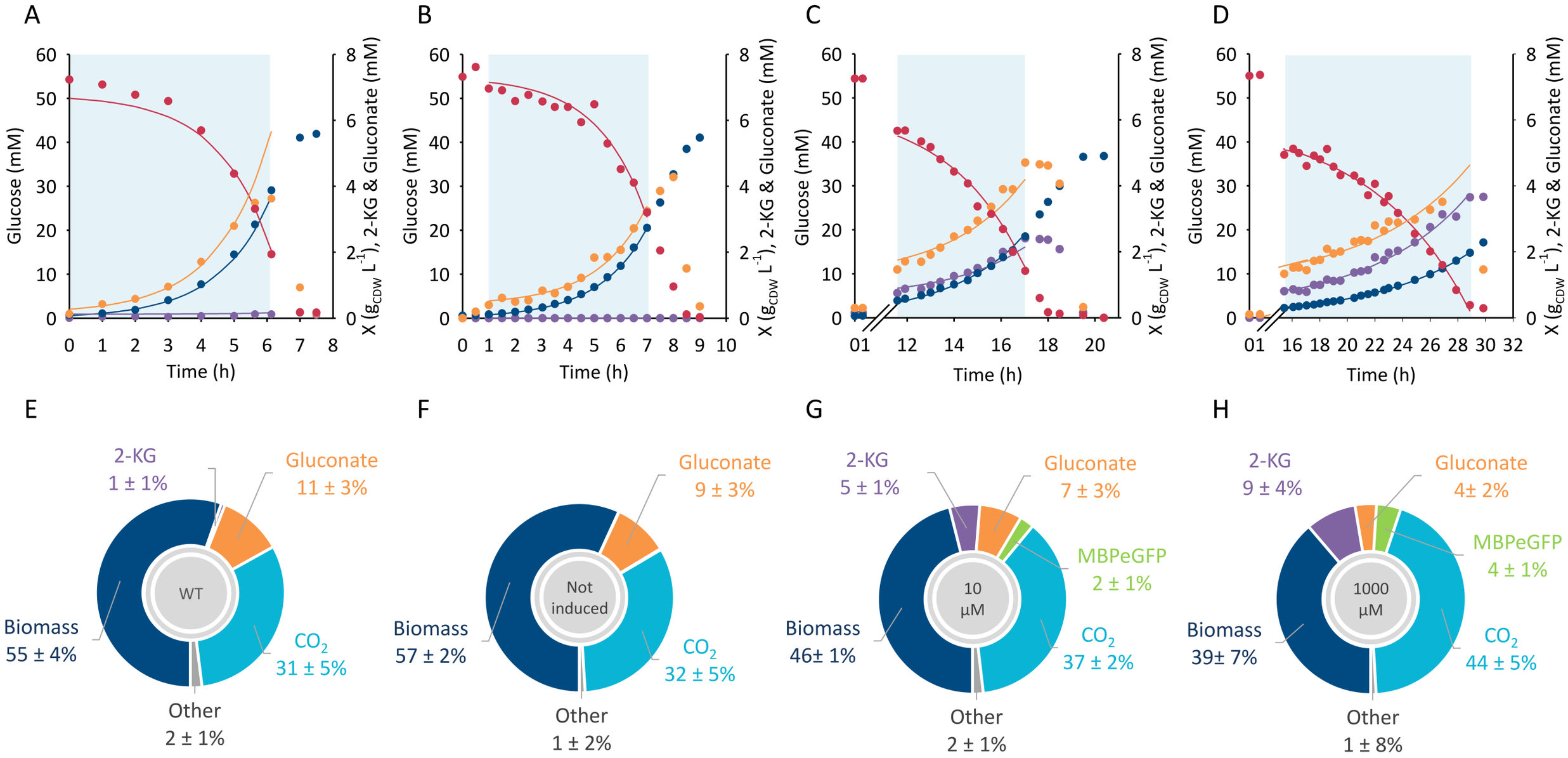
A
B
C
D
Glucose (mM)
X (g_{CDW} L^{-1}), 2-KG & Gluconate (mM)
Time (h)
E
F
G
H
WT
Not induced
10 µM
1000 µM
2-KG
1 ± 1%
Gluconate
11 ± 3%
Biomass
55 ± 4%
CO_2
31 ± 5%
Other
2 ± 1%
Gluconate
9 ± 3%
Biomass
57 ± 2%
CO_2
32 ± 5%
Other
1 ± 2%
2-KG
5 ± 1%
Gluconate
7 ± 3%
MBPeGFP
2 ± 1%
Biomass
46± 1%
CO_2
37 ± 2%
Other
2 ± 1%
2-KG
9 ± 4%
Gluconate
4± 2%
MBPeGFP
4 ± 1%
Biomass
39± 7%
CO_2
44 ± 5%
Other
1 ± 8%

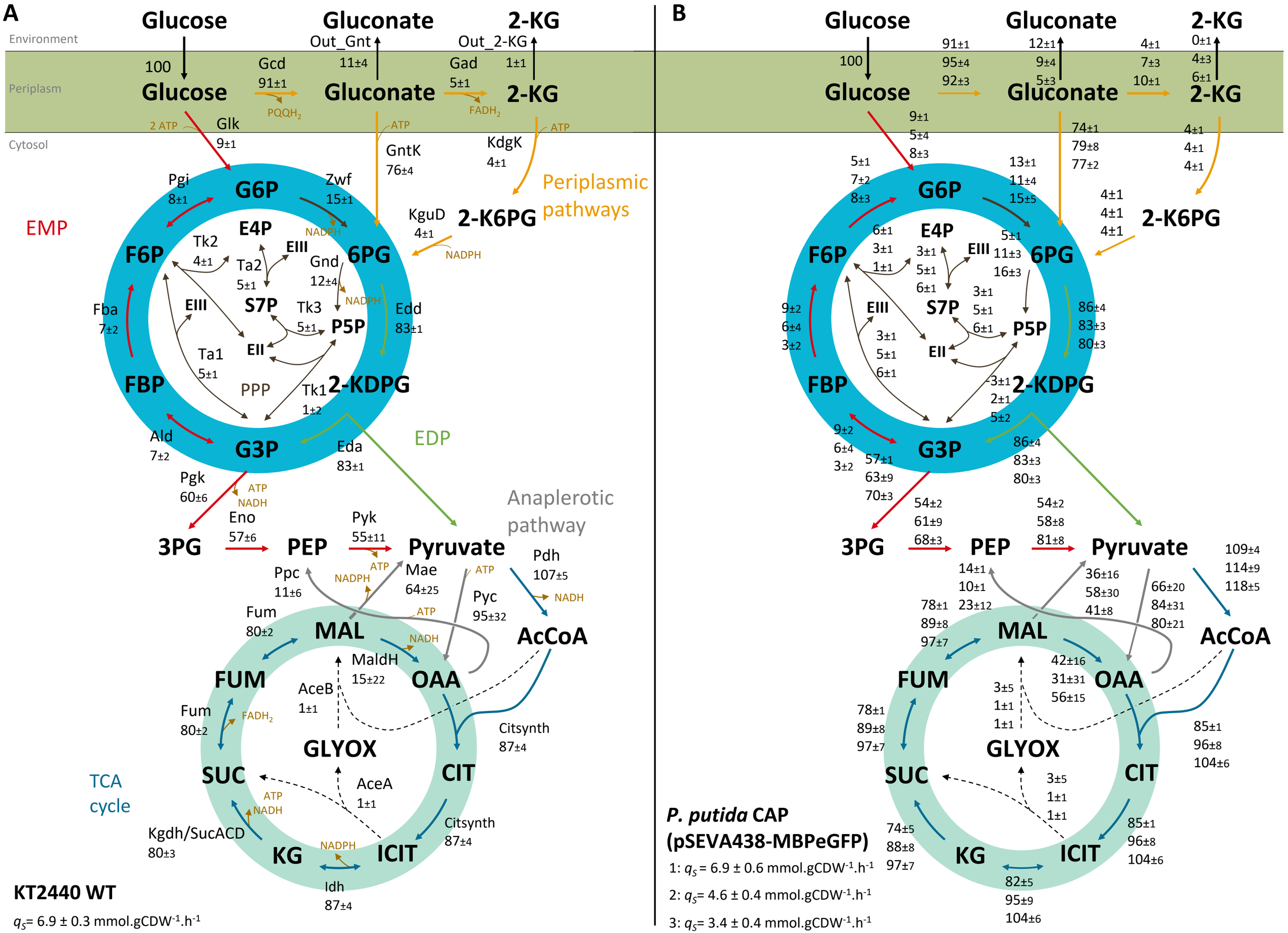
A
Environment
Periplasm
Cytosol
Glucose
Gluconate
2-KG
100
Out_Gnt
11±4
Out_2-KG
1±1
Gcd
91±1
PQQH2
Gad
5±1
FADH2
Glucose
Gluconate
2-KG
2 ATP
Glk
9±1
ATP
GntK
76±4
ATP
KdgK
4±1
Periplasmic pathways
KguD
4±1
2-K6PG
NADPH
EMP
Pgi
8±1
G6P
Zwf
15±1
NADPH
E4P
Tk2
4±1
EIII
Ta2
5±1
Gnd
12±4
NADPH
F6P
6PG
EIII
S7P
Tk3
5±1
P5P
Fba
7±2
Edd
83±1
EII
Ta1
5±1
FBP
PPP
Tk1
1±2
2-KDPG
Ald
7±2
G3P
Eda
83±1
EDP
Pgk
60±6
ATP
NADH
Anaplerotic pathway
Eno
57±6
Pyk
55±11
3PG
PEP
Pyruvate
Ppc
11±6
NADPH
ATP
Mae
64±25
ATP
Pdh
107±5
NADH
Pyc
95±32
Fum
80±2
ATP
MAL
NADH
AcCoA
MaldH
15±22
FUM
OAA
AceB
1±1
Fum
80±2
FADH2
Citsynth
87±4
GLYOX
TCA cycle
SUC
CIT
AceA
1±1
ATP
NADH
Citsynth
87±4
Kgdh/SucACD
80±3
KG
NADPH
ICIT
Idh
87±4
KT2440 WT
qS= 6.9 ± 0.3 mmol.gCDW-1.h-1
B
Glucose
Gluconate
2-KG
100
91±1
95±4
92±3
12±1
9±4
5±3
4±1
7±3
10±1
0±1
4±3
6±1
Glucose
Gluconate
2-KG
9±1
5±4
8±3
74±1
79±8
77±2
4±1
4±1
4±1
5±1
7±2
8±3
13±1
11±4
15±5
4±1
4±1
4±1
2-K6PG
G6P
6±1
3±1
1±1
E4P
3±1
5±1
6±1
EIII
5±1
11±3
16±3
F6P
6PG
9±2
6±4
3±2
EIII
S7P
3±1
5±1
6±1
86±4
83±3
80±3
P5P
3±1
5±1
6±1
EII
FBP
-3±1
2±1
5±2
2-KDPG
9±2
6±4
3±2
G3P
57±1
63±9
70±3
86±4
83±3
80±3
54±2
61±9
68±3
54±2
58±8
81±8
3PG
PEP
Pyruvate
109±4
114±9
118±5
14±1
10±1
23±12
36±16
58±30
41±8
66±20
84±31
80±21
78±1
89±8
97±7
MAL
AcCoA
42±16
31±31
56±15
FUM
OAA
3±5
1±1
1±1
78±1
89±8
97±7
85±1
96±8
104±6
GLYOX
SUC
CIT
3±5
1±1
1±1
74±5
88±8
97±7
85±1
96±8
104±6
KG
ICIT
82±5
95±9
104±6
P. putida CAP
(pSEVA438-MBPeGFP)
1: qS = 6.9 ± 0.6 mmol.gCDW-1.h-1
2: qS= 4.6 ± 0.4 mmol.gCDW-1.h-1
3: qS= 3.4 ± 0.4 mmol.gCDW-1.h-1

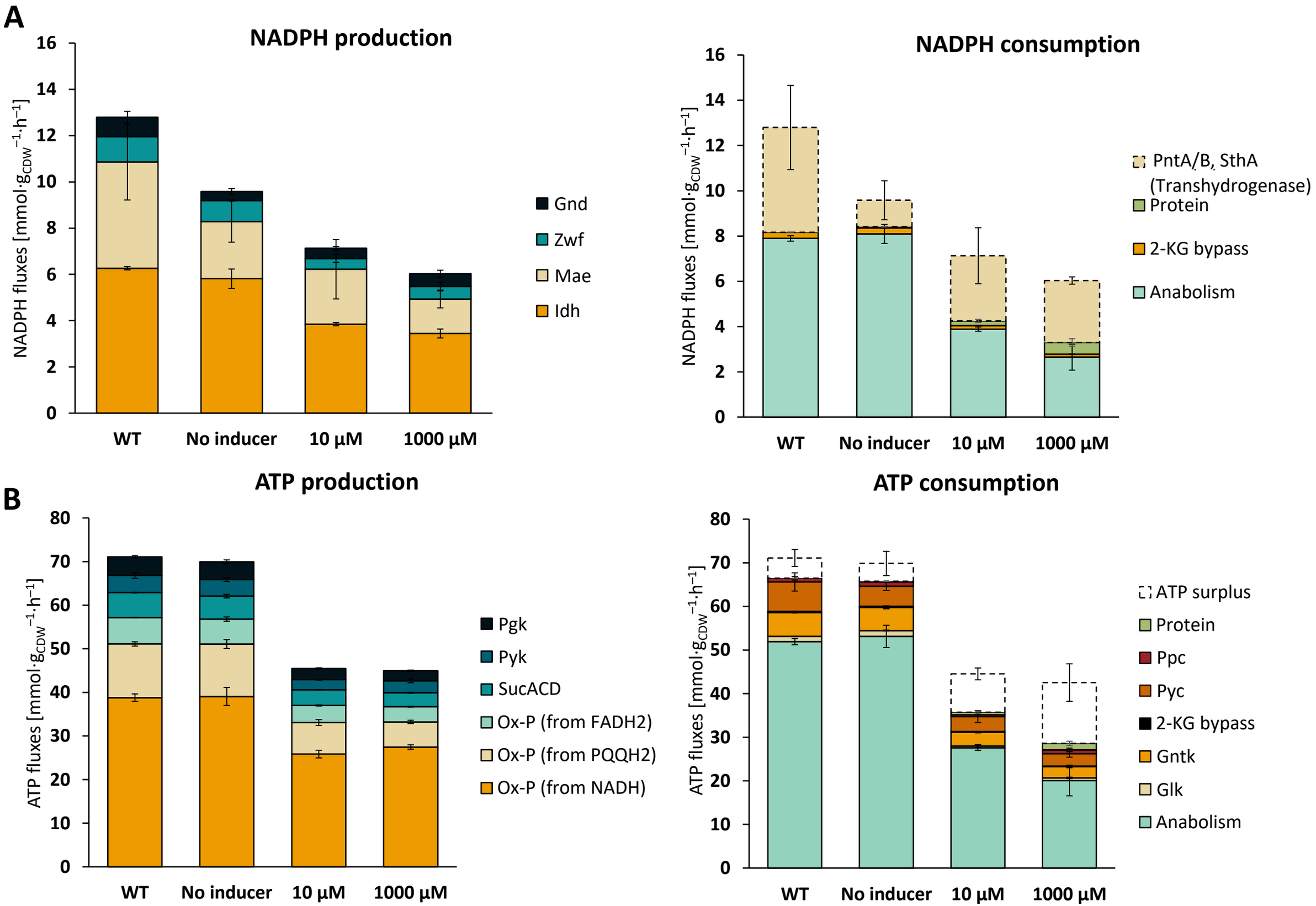
A
NADPH production
NADPH fluxes [mmol·g$_{CDW}^{-1}$·h^{-1}]
0
2
4
6
8
10
12
14
16
WT
No inducer
10 µM
1000 µM
Gnd
Zwf
Mae
Idh
NADPH consumption
PntA/B, SthA (Transhydrogenase)
Protein
2-KG bypass
Anabolism
B
ATP production
ATP fluxes [mmol·g$_{CDW}^{-1}$·h^{-1}]
0
10
20
30
40
50
60
70
80
Pgk
Pyk
SucACD
Ox-P (from FADH2)
Ox-P (from PQQH2)
Ox-P (from NADH)
ATP consumption
ATP surplus
Protein
Ppc
Pyc
2-KG bypass
Gntk
Glk
Anabolism

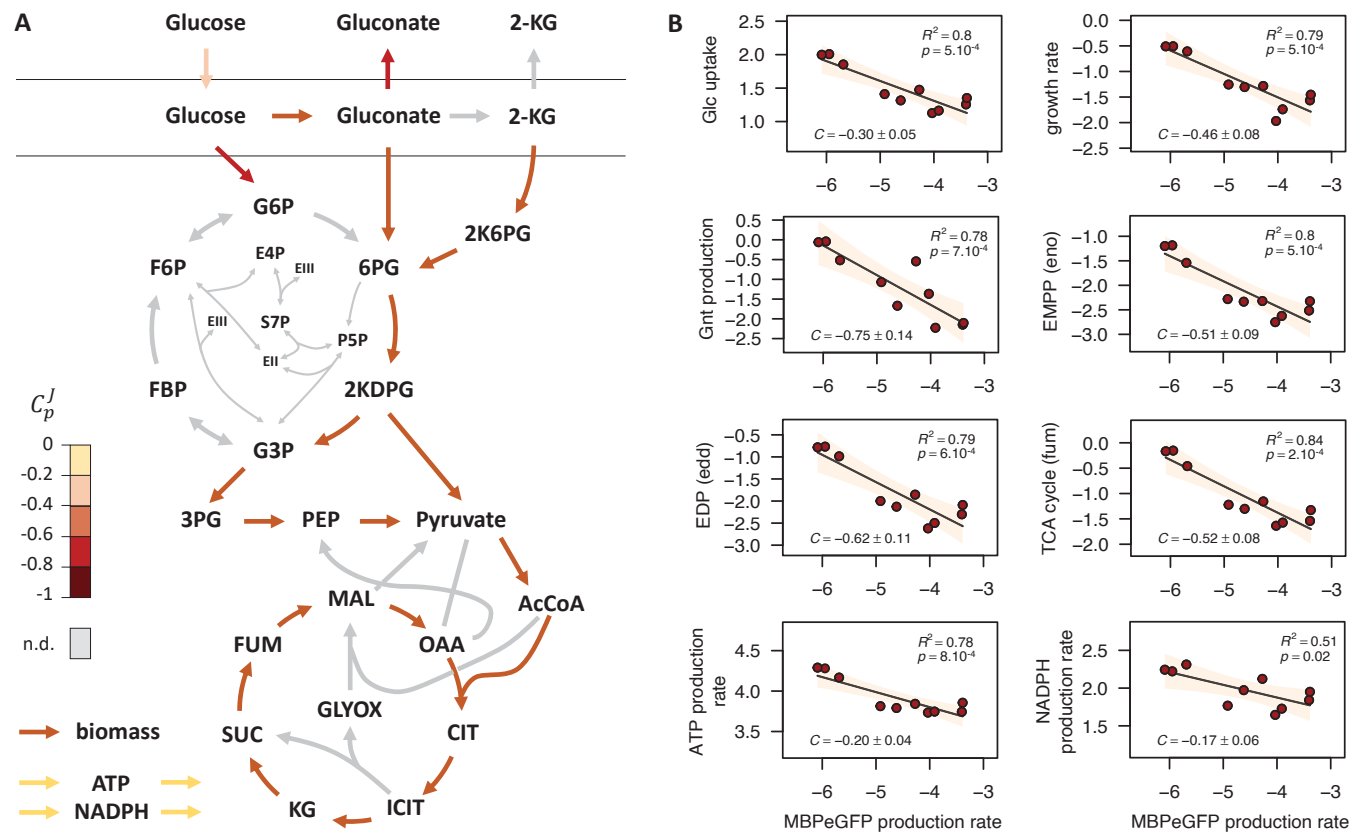
A
Glucose
Gluconate
2-KG
Glucose
Gluconate
2-KG
G6P
2K6PG
F6P
E4P
EIII
6PG
EIII
S7P
P5P
EII
FBP
2KDPG
G3P
3PG
PEP
Pyruvate
MAL
AcCoA
FUM
OAA
GLYOX
SUC
CIT
KG
ICIT
C_p^J
0
-0.2
-0.4
-0.6
-0.8
-1
n.d.
biomass
ATP
NADPH
B
Glc uptake
$R^2 = 0.8$
$p = 5.10^{-4}$
$C = -0.30 \pm 0.05$
growth rate
$R^2 = 0.79$
$p = 5.10^{-4}$
$C = -0.46 \pm 0.08$
Gnt production
$R^2 = 0.78$
$p = 7.10^{-4}$
$C = -0.75 \pm 0.14$
EMPP (eno)
$R^2 = 0.8$
$p = 5.10^{-4}$
$C = -0.51 \pm 0.09$
EDP (edd)
$R^2 = 0.79$
$p = 6.10^{-4}$
$C = -0.62 \pm 0.11$
TCA cycle (fum)
$R^2 = 0.84$
$p = 2.10^{-4}$
$C = -0.52 \pm 0.08$
ATP production rate
$R^2 = 0.78$
$p = 8.10^{-4}$
$C = -0.20 \pm 0.04$
NADPH production rate
$R^2 = 0.51$
$p = 0.02$
$C = -0.17 \pm 0.06$
MBPeGFP production rate
MBPeGFP production rate